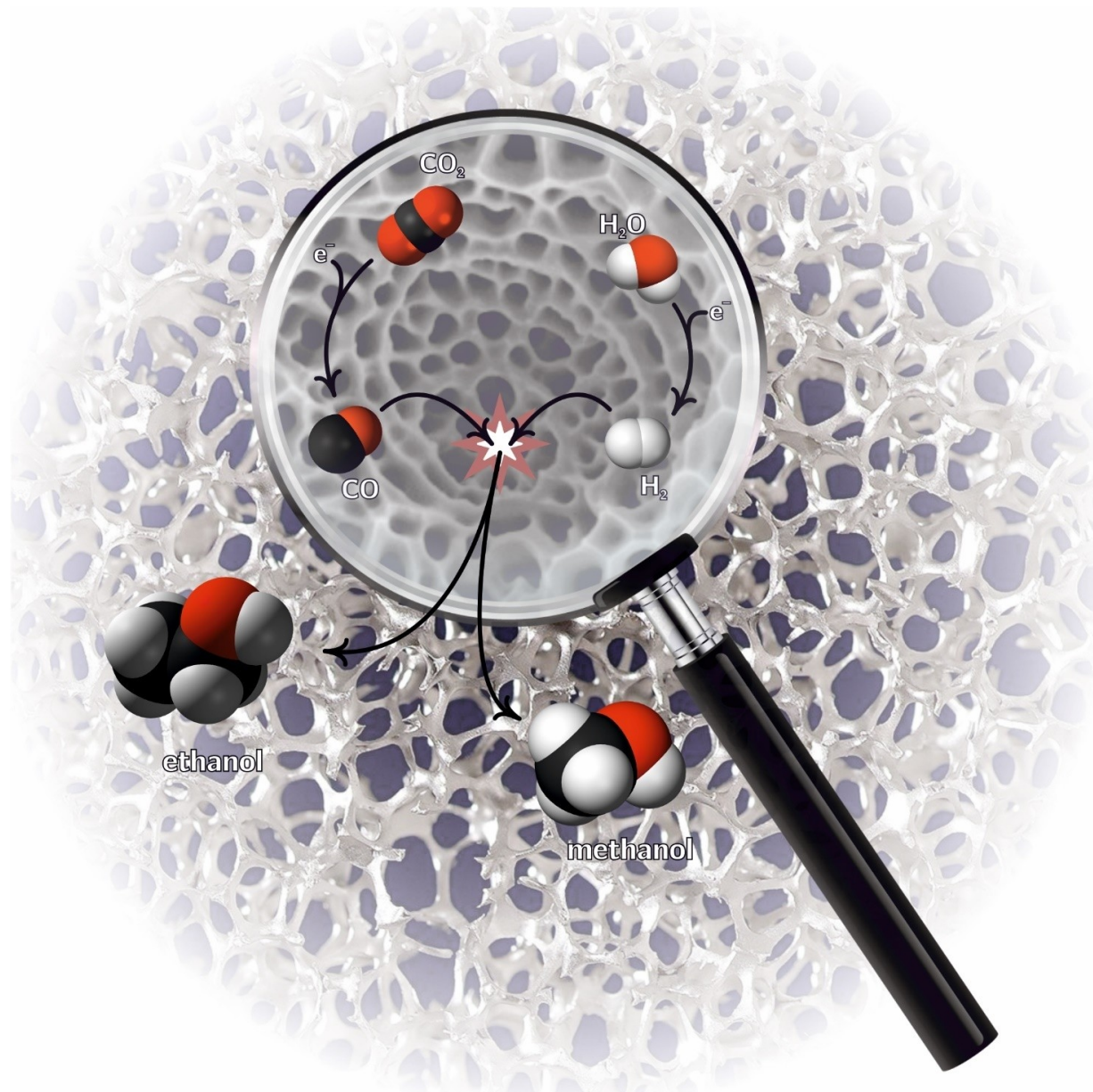


# Hydrogen Bubble Templated Metal Foams as Efficient Catalysts of CO<sub>2</sub> Electroreduction

Soma Vesztegom,<sup>\*[a, b]</sup> Abhijit Dutta,<sup>[a]</sup> Motiar Rahaman,<sup>[a]</sup> Kiran Kiran,<sup>[a]</sup>  
Iván Zelocualtecatl Montiel,<sup>[a]</sup> and Peter Broekmann<sup>\*[a]</sup>



The creation of open porous structures with an extremely high surface area is of great technological relevance. The electrochemical deposition of metal foams around co-generated hydrogen bubbles that act as templates for the deposition is a promising, cheap and simple approach to the fabrication of new electrocatalyst materials. Metal foams obtained by dynamic hydrogen bubble templating (DHBT) offer an intrinsically high electrical conductance with an open porous structure that enables the fast transport of gases and liquids. As an additional

benefit, the confined space within the pores of DHBT metal foams may act as small reactors that can harbour reactions not possible at an open electrode interface. The number, distribution, and size of the pores can be fine-tuned by an appropriate choice of the electrolysis parameters so that metal foam catalysts prepared by the DHBT technique meet certain requirements. In this paper, we review the preparation of certain metal foams, and their applications as catalysts for the electrochemical reduction of CO<sub>2</sub>.

## 1. Introduction

The rising concentration of atmospheric carbon dioxide (CO<sub>2</sub>) and its consequences on climate and related societal changes present a major challenge to humankind, necessitating the development of industries with a zero, or possibly negative, CO<sub>2</sub> footprint.<sup>[1]</sup> Electrochemical technologies provide an attractive solution to the problem, where electrons preferably gained from a renewable energy source can be used to turn CO<sub>2</sub> into value-added products.<sup>[2]</sup> Technologies already exist to achieve this goal, although their operation is still far from perfect. A key factor of developing CO<sub>2</sub> electrolysis technologies was, and probably still remains, the invention of new catalytic electrode materials. The application of proper catalysts can ensure higher yield and also a tailored selectivity toward the formation of certain sought-after products.

At recent technological levels, the most desired products of CO<sub>2</sub> electroreduction are syngas (a mixture of CO and H<sub>2</sub>); C<sub>2</sub> hydrocarbons (primarily, C<sub>2</sub>H<sub>4</sub>); short carbon chain alcohols (like methanol, ethanol or propanol); and formate or formic acid. The formation of other products by electrochemical CO<sub>2</sub> reduction (e.g., that of methane) would also be possible, but considering current market prices, the above aims are the ones that remain economically viable.<sup>[3]</sup>

Electrocatalysis plays a central role in lowering the energy barrier and thereby increasing the yield and decreasing the cost of CO<sub>2</sub> electroreduction, and in assuring that the reaction results in the desired product. Many efforts have thus been made to improve the performance of electrocatalysts, such as increasing

the surface area, improving the intrinsic activity of the active sites, and manipulating the transport of reactants and products to and from the electrode surface.<sup>[4]</sup> Among these methods, the fabrication of three-dimensional porous structures (i.e., metal foams<sup>[5]</sup>) and the application of these as electrode materials was proven to be an attractive way to improve electrocatalytic performance.<sup>[6]</sup>

The application of metal foams as electrocatalysts is advantageous, as self-standing foams can directly be employed as working electrodes, often without the need of additional mechanical support. They offer a large surface area that is not only accessible to reactants, but also enables fast, multi-dimensional electron transport pathways.<sup>[6,7]</sup> Also, metal foams can act as a support for other catalysts, rendering the application of conductive binders, like Nafion, unnecessary in catalyst design.

According to IUPAC,<sup>[8]</sup> "a foam is a dispersion in which a large proportion of gas by volume in the form of gas bubbles, is dispersed in a liquid, solid or gel." Foams can either be open-cell or closed-cell structured; for the purposes of electrocatalysis, foams with open-cell structures are the most useful.<sup>[9]</sup> Several non-electrochemical<sup>[10]</sup> and electrochemical<sup>[9]</sup> methods have been described for the preparation of metal foams, mainly including selective dissolution,<sup>[11–14]</sup> templating,<sup>[15,16]</sup> combustion,<sup>[17,18]</sup> and the sol-gel method.<sup>[19,20]</sup> Synthesis and characterization strategies of noble metal foams prepared by these methods, as well as their application for electrocatalysis purposes, were recently reviewed in detail by the Eychmüller group<sup>[9,20]</sup> and by Zhu *et al.*<sup>[6]</sup> A relatively newly developed, yet very promising method of the preparation of metal foams namely, dynamic hydrogen bubble templated (DHBT) electrodeposition<sup>[22]</sup> was, however, not addressed in these works. The aim of this survey is to fill this gap, and to review, in details, the use of DHBT for the preparation of metal foams that can be used, primarily, as electrocatalysts for CO<sub>2</sub> reduction.


## 2. DHBT Based Preparation of Metal Foams


### 2.1. General Considerations

When electrodepositing noble (e.g., Au, Pt, Ag, Cu), or especially base metals (e.g., Zn, Co, Fe, Ni) from solutions of their salts, concurrent hydrogen evolution is usually considered as a major problem that causes ramification of the deposited metal layer and accounts for often undesired changes in its mechanical and

[a] Dr. S. Vesztergom, Dr. A. Dutta, Dr. M. Rahaman, K. Kiran, I. Zelocualtecatl Montiel, Prof. P. Broekmann  
Department of Chemistry and Biochemistry  
University of Bern  
Freiestraße 3  
Bern 3012 (Switzerland)  
E-mail: peter.broekmann@dcb.unibe.ch  
vesztergom@chem.elte.hu

[b] Dr. S. Vesztergom  
Department of Physical Chemistry  
Eötvös Loránd University  
Pázmány Péter sétány 1/A  
Budapest 1117 (Hungary)

 This publication is part of a Special Collection on "Catalysis in Confined Spaces". Please check the ChemCatChem homepage for more articles in the collection.

 © 2020 The Authors. ChemCatChem published by Wiley-VCH GmbH. This is an open access article under the terms of the Creative Commons Attribution License, which permits use, distribution and reproduction in any medium, provided the original work is properly cited.

optical properties, sometimes impairing the entire process.<sup>[26]</sup> Dynamic hydrogen bubble templating (DHBT) serves as a glaring counter-example, where the loss of some current due to hydrogen evolution is turned to a benefit, as the formed hydrogen bubbles aid the creation of spongy, high surface area metal foams that can be extremely useful for the purposes of electrocatalysis.

The co-generation of hydrogen along with metal deposition, in order to create high surface area electrode materials, has been part of the arsenal of electrochemists for quite some time now; *e.g.*, this was the method used for the creation of platinum black in the original recipe of Lummer and Kurlbaum<sup>[23]</sup> and of Kohlrusch<sup>[24]</sup> (Figure 1). Starting with the advent of the 21st century, the method experienced a boom, as it turned out to be quite useful for the creation of high surface area electrocatalyst materials – not necessarily platinum based ones. Among recent works directed at the development of tailored electrocatalyst materials using the DHBT method, the works of Chialvo and Marozzi,<sup>[27,28]</sup> Shin *et al.*,<sup>[29,30]</sup> Nikolić *et al.*,<sup>[31–36]</sup> Cherevko *et al.*,<sup>[37–43]</sup> as well as the works of the Bhargava group,<sup>[44–47]</sup> including a review<sup>[22]</sup> deserve further attention.

In principle, there are two processes underlying the DHBT method that play a crucial role in the fabrication of metal

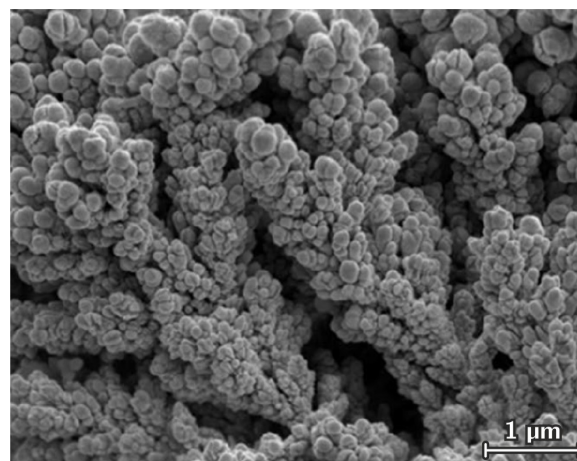


**Figure 1.** Scanning electron micrograph of platinum black, electrochemically deposited on a Pt surface from a hexachloroplatinate solution, using the recipe of Lummer and Kurlbaum<sup>[23]</sup> modified by Kohlrusch.<sup>[24]</sup> Reproduced from Ref. 25 with the permission of Nature.

foams. One is Reaction (R1), the deposition of the metal from a solution of its salt:



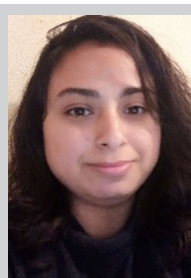
Soma Vesztergom obtained his M.Sc. (2010) and Ph.D. (2014) degrees in chemistry at Eötvös Loránd University of Budapest, Hungary. He was a post-doctoral researcher in Peter Broekmann's group at the University of Bern for a year (2014) and is a regular collaborator of this group since then. His research primarily focuses on instrumental developments in electrochemistry and on the modelling of electrocatalytic processes. Currently, he is an assistant professor at Eötvös Loránd University in Budapest.



Abhijit Dutta obtained his Ph.D in chemistry from the Indian Institute of Engineering Science and Technology, Kolkata. He worked as a post-doctoral fellow at the National University of Singapore. Afterwards, he joined the interfacial electrochemistry group of Peter Broekmann at the University of Bern, Switzerland. His research is focused on the development of various operando spectroscopies (Raman, XAS, and XRD) to characterize novel electrocatalysts for the selective conversion of CO<sub>2</sub> to value-added products.



Motiar Rahaman obtained his M.Sc. degree in chemistry at the Indian Institute of Technology Madras, Chennai (2013) and his Ph.D. (2018) at the University of Bern. The topic of his Ph.D. thesis was the electrochemical conversion of CO<sub>2</sub> into value-added products. Currently he is a post-doctoral researcher at the University of Cambridge.



Kiran obtained her M.Sc. degree in physics at the Maharshi Dayanand University in Rohtak, India, in 2015 and currently pursues a Ph.D. in Peter Broekmann's research group at the University of Bern. Her primary research interests are in the preparation of nanomaterials and the application of these as catalysts for CO<sub>2</sub> electroreduction.



Ivan Zelocualtecatl Montiel received his B.Sc. and M.Sc. in Chemistry from the Meritorious Autonomous University of Puebla, Mexico, in 2013 and 2016, respectively. He is currently a Ph.D. candidate in the Department of Chemistry and Biochemistry at the University of Bern, under the supervision of Prof. Dr. Peter Broekmann. His research interest is focused on the development of novel catalysts for CO<sub>2</sub> electroreduction.



Peter Broekmann obtained his M.Sc. in chemistry (1998) and a Ph.D. (2000) from the University of Bonn, Germany. After a post-doctoral stay in 2001 at the University of Twente he became project leader at the Institute of Physical Chemistry in Bonn. Since 2008, Prof. Dr. Broekmann is lecturer for electrochemistry at the University of Bern (Switzerland). His research focuses on metal deposition processes for semiconductor and electrocatalysis applications.

The other is the hydrogen evolution reaction (HER) that in an acidic solution is supposed to proceed by Reaction (R2),



while in solutions of  $\text{pH} > 7$ , the primary source of hydrogen is the electroreduction of water itself:



Although for the preparation of metal foams using the DHBT technique, usually acidic solutions are applied, it has to be noted that under harsh cathodic conditions the surroundings of the electrode surface quickly get depleted in  $\text{H}^+$ , in which case direct water reduction, Reaction (R3), cannot be ignored.<sup>[48]</sup>

The fundamental idea of DHBT is that the  $\text{H}_2$  bubbles generated in Reactions (R2) and (R3) disrupt the growth of the metal layer, acting as a dynamic template for the electro-deposition process. Micropores in the submicron range and macropores in the 10–100  $\mu\text{m}$  size range are formed as a result of the growth of metal around small or coalesced bubbles generated on the surface, blowing up the specific surface area.<sup>[22]</sup>

When applying the DHBT method, high cathodic overpotentials are used, so that the rates of Reactions (R1) and (R2)–(R3) become comparable and decisive for the obtained foam structure. Apart from the reaction rates, however, other factors such as the nucleation, growth and detachment of the surface-generated bubbles, the intensive stirring and the related convective effects caused by bubble formation, the local alkalination of the near-electrode solution layers and its consequences on the chemistry of metal deposition, complex formation, the action of additives, etc. may also determine the surface morphology of the deposited foam. Below, we give a summary of these effects.

## 2.2. Mechanistic Aspects

In an excellent work, Nikolić<sup>[35]</sup> treats DHBT following Winand's classification of metals,<sup>[49]</sup> and shows contrary to previous claims<sup>[51]</sup> that metals from all three Winand groups can be obtained in three dimensional foam forms under the appropriate electrodeposition conditions. According to Winand, metals can be classed in the following three groups (Figure 2): *i.*) normal metals (such as Cd, Zn, Sn, Ag) that are characterized by low melting points, high ( $j_{0,\text{dep}} > 100 \text{ A cm}^{-2}$ ) exchange current densities of metal deposition and low catalytic activities for hydrogen evolution; *ii.*) intermediate metals (such as Au, Cu and Ag, if in the case of Ag, deposition occurs from the solution of a complex and not of free  $\text{Ag}^+$  ions) that are characterized by moderate melting points, intermediate ( $1 \text{ A cm}^{-2} \leq j_{0,\text{dep}} \leq 100 \text{ A cm}^{-2}$ ) exchange current densities of metal deposition and relatively low catalytic activities for hydrogen evolution; and *iii.*)

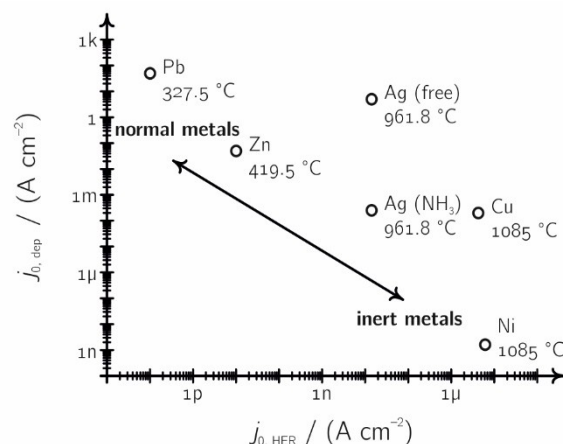


**Figure 2.** According to Winand,<sup>[49]</sup> metals can be classed into three groups (normal, intermediate and inert) based on their  $j_{0,\text{dep}}$  DEBHT exchange current densities and melting points. In his treatise on DHBT,<sup>[35]</sup> Nikolić extends Winand's original classification<sup>[49]</sup> based on the  $j_{0,\text{HER}}$  exchange current density of HER. The graph shown here was created using data obtained from Refs. 50 and 36.

inert metals (such as Fe, Ni, Co, Pt, Cr, Mn) that have high melting points, low ( $j_{0,\text{dep}} < 1 \text{ A cm}^{-2}$ ) exchange current densities of metal deposition and relatively high catalytic activities for hydrogen evolution.

In case of each three metal groups, the success of DHBT in creating metal foams depends on whether on the given metal, hydrogen is forming large enough bubbles (that is mostly a question of nucleation and growth kinetics and of surface thermodynamics) and on whether the rate of metal deposition is high enough to allow deposited dendritic metal structures to overgrow a hydrogen bubble, before it leaves the electrode surface.

As shown by Popov *et al.*,<sup>[53]</sup> in case of metals with low or moderate  $j_{0,\text{dep}}$  values, dendrite formation is possible only if the deposition overpotential  $\eta$  exceeds a minimum initiation overpotential

$$\eta_{\text{ini}} = -\frac{RT j_{\text{lim,dep}}}{zF j_{0,\text{dep}}} \quad (1)$$

where  $j_{\text{lim,dep}}$  is the effective limiting current density of metal deposition. Note that the value of  $j_{\text{lim,dep}}$  strongly depends on the prevailing hydrodynamic conditions and the vigorous mixing of the near-electrode solution caused by HER.

While for metal depositions in quiescent systems, the thickness of the diffusion layer of metal ions can (over time) extend to even a few hundreds of micrometers, it was shown that for quickly gas evolving electrodes (volumetric gas evolution rate normalized to surface area:  $100 \text{ cm}^3 \text{ min}^{-1}$ , corresponding to hydrogen evolution occurring with a current density of about  $5 \text{ A cm}^{-2}$ ), the diffusion layer becomes only a few micrometers thick and the coverage of the surface by gas bubbles can exceed 30%.<sup>[54]</sup> Thus, at electrodes that evolve hydrogen at a high rate, due to the decrease of the diffusion

layer thickness and the corresponding increase of  $j_{\text{lim,depr}}$  the "effective overpotential" (a term coined by Nikolić *et al.*<sup>[31]</sup>) may be lower than what is required for efficient dendrite formation.

What was said above is nicely demonstrated in Ref. 31 for the deposition of honeycomb-like copper foams on plane copper substrates from an aqueous solution containing  $0.10 \text{ mol dm}^{-3} \text{ CuSO}_4$  and  $0.50 \text{ mol dm}^{-3} \text{ H}_2\text{SO}_4$ . In Figure 3 we can observe the following: *i.*) that at  $\eta = -0.550 \text{ V}$ , a value that falls inside the limiting current density of copper deposition where no hydrogen evolution takes place, cauliflower-like agglomerates of copper grains were formed; *ii.*) that at  $\eta = -0.700 \text{ V}$ , just outside the limiting current region of copper deposition, where the Faradaic efficiency of HER is only about 5%, branch-like three dimensional dendrites are formed; and finally *iii.*) that at  $\eta = -0.800$  or  $-1.000 \text{ V}$ , holes formed of detached hydrogen bubbles surrounded by cauliflower-like agglomerates of copper grains are seen.

It is important to note with respect to the depositions occurring at high overpotentials that the number of holes formed at  $-1.000 \text{ V}$  is larger than that at  $-0.800 \text{ V}$ , which is due to the higher Faradaic efficiency of hydrogen evolution (almost 50% at  $-1.000 \text{ V}$  and about 30% at  $-0.800 \text{ V}$ ). As communi-

cated by Nikolić *et al.* elsewhere,<sup>[32]</sup> the critical Faradaic efficiency that hydrogen evolution should achieve in order to create hydrodynamic conditions that favour foam formation is 10% for copper depositing baths with a  $\text{CuSO}_4$  concentration of  $0.15 \text{ mol dm}^{-3}$  and less, in  $0.5 \text{ mol dm}^{-3} \text{ H}_2\text{SO}_4$ .

### 2.3. Creating Metal Foams with Hierarchic Porosity: The Effect of Deposition Time

As shown in Figure 4, at the initial stages (after the first 10 seconds) of the potentiostatic preparation of copper foams ( $\eta = -1.000 \text{ V}$ ,  $c_{\text{CuSO}_4} = 0.1 \text{ mol dm}^{-3}$ ,  $c_{\text{H}_2\text{SO}_4} = 0.5 \text{ mol dm}^{-3}$ ), nucleation sites of  $\text{H}_2$  bubbles and surrounding agglomerates of copper grains are already visible. Hydrogen evolution is initiated at irregularities of the surface, where small bubbles are formed, grow to a certain size and are then detached. The higher the current density, the more nucleation sites become active, and also the rate of growth of the bubbles increases. While at lower current densities, only the surface irregularities are active, at higher current densities bubbles are also formed on the more homogeneous parts of the surface.<sup>[56]</sup> After

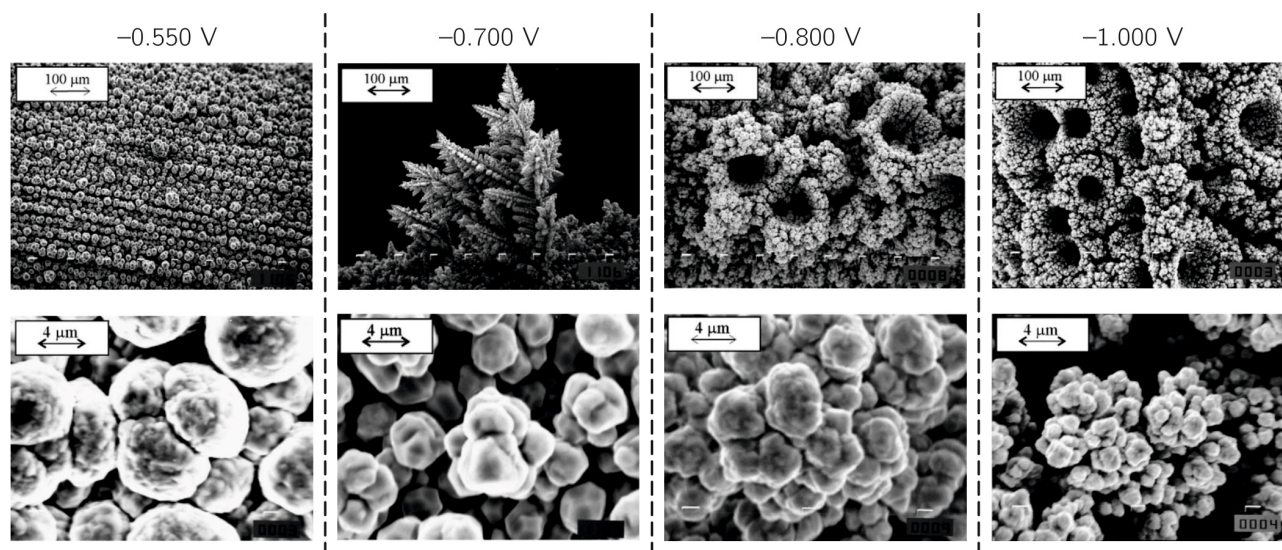


**Figure 3.** Morphologies of Cu deposits obtained after 60 s of potentiostatic electrolysis, at different values of the deposition overpotential from an aqueous solution containing  $0.10 \text{ mol dm}^{-3} \text{ CuSO}_4$  and  $0.50 \text{ mol dm}^{-3} \text{ H}_2\text{SO}_4$ . Reproduced from Ref. 31 with the permission of Elsevier.

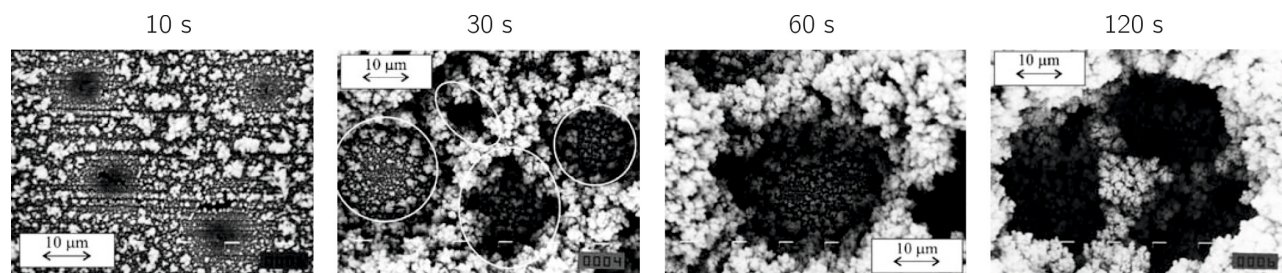


**Figure 4.** Morphologies of Cu deposits obtained after different times of potentiostatic electrolysis at a deposition overpotential of  $-1.000 \text{ V}$ , from an aqueous solution containing  $0.10 \text{ mol dm}^{-3} \text{ CuSO}_4$  and  $0.50 \text{ mol dm}^{-3} \text{ H}_2\text{SO}_4$ . Reproduced from Ref. 34 with the permission of Springer.

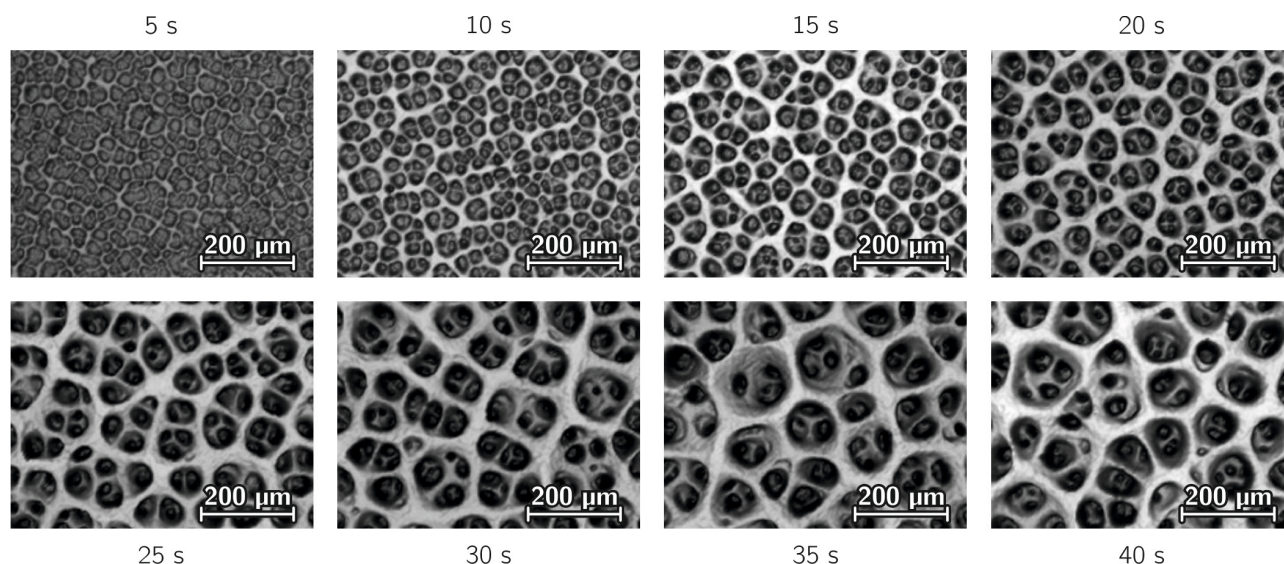


**Figure 5.** Morphologies of Cu deposits obtained after different times of galvanostatic electrolysis at  $-2.0 \text{ A cm}^{-2}$ , from an aqueous solution containing  $0.20 \text{ mol dm}^{-3} \text{ CuSO}_4$  and  $1.0 \text{ mol dm}^{-3} \text{ H}_2\text{SO}_4$ . Reproduced from Ref. 52 with permission of The Electrochemical Society.

30 seconds of potentiostatic electrolysis (Figure 4) we can notice that the deposited copper grows around the hydrogen bubbles that remained adherent to the surface, forming regular (circle-shaped) and irregular (from top view, ellipse shaped) cavities. As shown in Figure 5, an even more pronounced hierarchy is achieved if instead of potentiostatic control, we apply galvanostatic electrodeposition of foamed copper.<sup>[52]</sup>

As evident in Figures 3 and 4, the deposited metal foams exhibit two types of porosity: they show macropores, formed by the larger, coalesced bubbles; and micropores (porosities within the walls of the macropores) that are created as channels by the vigorous formation of small hydrogen bubbles over the copper dendrites.<sup>[34]</sup> As the electrolysis proceeds, the size of the macropores tends to increase, yielding a hierarchically structured foam deposit that has a bigger number of small pores close to the substrate, and fewer but bigger-sized pores close to the solution interface (Figures 6 and 7). This graded structure is ideally suited for the preparation of electrocatalyst materials with pore sizes specifically tuned by the selection of appropriate deposition times.<sup>[30]</sup>

## 2.4. Further Factors Affecting Foam Structure

As pointed out by Nikolić,<sup>[35]</sup> the formation of porous structures is possible for metals of all three Winand classes, provided that the deposition overpotential that is either directly applied or established as a result of galvanostatic polarization, exceeds the minimum initiation overpotential  $\eta_{\text{inir}}$  defined by Equation (1), and that at this overpotential, hydrogen production is already vigorous.

Intensive hydrogen evolution will then have two effects: *i.*) that due to stirring the near-electrode solution, it decreases the thickness of the diffusion layer, increasing the limiting current

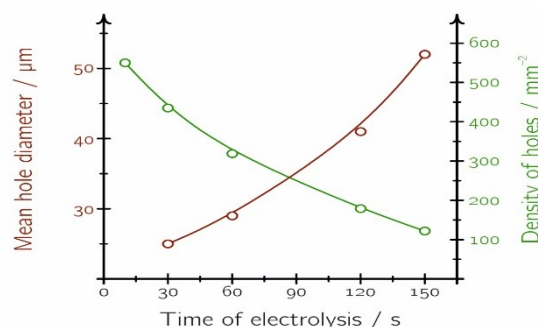


**Figure 6.** The size and number of  $\text{H}_2$  bubble templated holes in Cu deposits obtained at a deposition overpotential of  $-1.000 \text{ V}$ , from an aqueous solution containing  $0.10 \text{ mol dm}^{-3} \text{ CuSO}_4$  and  $0.50 \text{ mol dm}^{-3} \text{ H}_2\text{SO}_4$  are anti-correlated as the deposition proceeds. Graph created using data from Ref. 34.

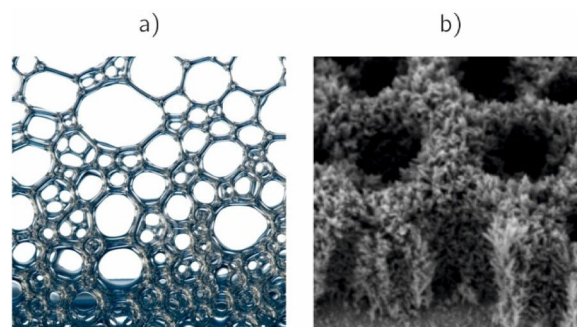


**Figure 7.** a) Illustration of the hierarchical porosity of metal foams and b) cross-sectional scanning electron micrographs of a potentiostatically obtained Cu foam deposit, reproduced from Ref. 30 with permission of the American Chemical Society.

density  $j_{\text{lim,dep}}$  of metal deposition; and *ii.*) that due to the at least, temporal adherence of the bubbles to the surface, it will increase the effective current density. In case  $\theta$  denotes the ratio of the surface (in a time average) blocked by bubbles, the effective current density will be  $1/(1-\theta)$  times bigger than the current density applied (that is the current normalized by the geometric surface area).<sup>[57]</sup>

When preparing metal foams, one must keep in mind that exchange current densities found in the literature (like those plotted in Figure 2) are concentration dependent quantities and values found in literature are usually (but not always) normalized to a unity concentration of the metal or  $\text{H}^+$  ions in the bulk solution (for metal deposition and HER, respectively). Thus, the overall electrolyte composition will have a strong effect on determining actual hydrogen evolution/metal deposition current ratios.<sup>[58]</sup> When preparing metal foams from noble metals, *e.g.*, from silver,<sup>[38]</sup> gold<sup>[40]</sup> or palladium salts,<sup>[43]</sup> a larger metal salt concentration in the bath may be required than, for example, when depositing normal metals such as Sn or Pb, or even intermediate metals like Cu.

The success of metal foams preparation lies however not only in whether the right current densities for metal deposition and hydrogen evolution are achieved. The morphology of the deposit, especially on the macroscale, will be determined by the maximum size that  $\text{H}_2$  bubbles formed during the electrolysis can reach before breaking off the surface, and also by the rate at which bubble growth occurs (Figure 8).<sup>[55,59]</sup>

The break-off diameter  $d$  was found to depend on the partial current density of hydrogen evolution  $j_{\text{HER}}$  according to the empirical formula

$$d = d_0 (1 + a j_{\text{HER}})^b \quad (2)$$

where the constants  $a \approx 0.2 \text{ m}^2 \text{ A}^{-1}$  and  $b \approx 0.45$  were determined by Vogt and Balzer<sup>[57]</sup> by fitting to experimental data; note that these constant values may be significantly different, depending on the system studied.

The parameter  $d_0$  in Equation (2) is the break-off diameter in a current-free case, the value of which can be estimated by using a simplified form of the Fritz equation:<sup>[60]</sup>

$$d_0 = 1.20 \vartheta \sqrt{\frac{\gamma}{g \rho}} \quad (3)$$

where  $g$  is the gravitational acceleration,  $\vartheta$  denotes the contact angle of the bubble on the electrode surface,  $\rho$  is the density of the solution, and  $\gamma$  is the interfacial stress of the gas/liquid interface. Both the contact angle  $\vartheta$  and the surface tension  $\gamma$

may vary as function of the applied electrode potential (and/or current),<sup>[61]</sup> as well as near-surface variations of the viscosity of the solution<sup>[62]</sup> may affect both the break-off diameter and the trajectory of bubbles leaving the electrode surface.

Additives affecting the surface energetics (either the solid/liquid or the gas/liquid interfacial stress, for example by preferential adsorption on one or both of these interfaces) may have a significant impact on both the macro- and the micro-porosity of the obtained deposit.<sup>[30]</sup> For example cationic surfactants like cetyltrimethylammonium bromide (CTAB), when used as additives in copper deposition baths, were shown to suppress the collision among hydrogen bubbles by specifically adsorbing on the gas/liquid interface. This leads to a mild rate of hydrogen evolution and smaller hydrogen bubbles, thus resulting in a smaller pore structure.<sup>[63]</sup> Eventually, it was also shown that CTAB can also be used to fine-tune the hydrophobicity of DHBT-deposited copper foams.<sup>[64]</sup>

Another important factor that has an effect on the structure of the finally obtained deposit is the concentration and form of available  $\text{H}^+$  sources present in the depositing solutions. This parameter is probably even more important than the pH, which is only related to the concentration of free  $\text{H}^+$  ions in the bulk solution. During intensive hydrogen evolution, however, when the near-electrode solution region gets alkalinized, additional  $\text{H}^+$  sources such as  $\text{NH}_4^+$  or citric acid can act as buffers, providing an excess amount of  $\text{H}^+$  as a reactant supply for HER. Naturally, at large negative applied overpotentials or currents, even the direct reduction of  $\text{H}_2\text{O}$  can serve as means of HER. While in this case it is the autoprotolysis reaction of water that has to be taken into account to describe HER current densities,<sup>[48]</sup> for buffered systems additional (buffer) equilibria must be considered.<sup>[58]</sup>

Near-surface alkalination may have an adverse effect on the nature of the obtained deposits; *e.g.*, it can lead to the formation of hydroxides of the metal to be deposited.<sup>[64]</sup> While the application of buffers as bath components may successfully circumvent this effect, one also has to consider that some buffer components (especially due to complex formation) may also have other, indirect effects on the foam deposition process. For example, in case  $\text{NH}_4^+$  ions are used as a buffer, the  $\text{NH}_3$  molecules formed in the (alkaline) near-surface layers of the electrolyte solutions may act as complexing agents for the deposited metal, hindering its deposition. Although some experimental results do confirm this assumption,<sup>[38]</sup> the possibilities of complex formation are only scarcely treated in the literature of DHBT metal foam deposition.<sup>[22]</sup>

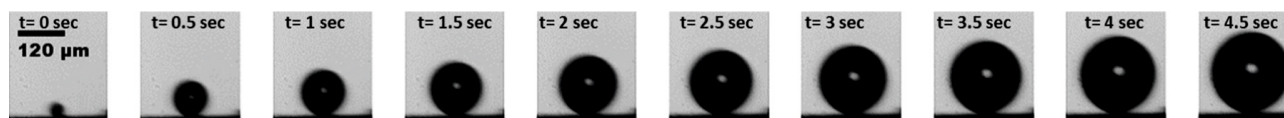


**Figure 8.** Sequence of images illustrating hydrogen bubble growth on an electrode surface at  $60 \text{ mA cm}^{-2}$  current density for HER. Reproduced from Ref. 55 with the permission of Elsevier.

## 2.5. Technical Challenges of DHBT Metal Foam Deposition

Although it is rarely mentioned in literature, one technical challenge that needs to be addressed with respect to DHBT metal foam deposition is the extreme high current that these methods require. Depositing hydrogen bubble templated metal foams necessitates the use of current densities in the range of 1 to 10 A cm<sup>-2</sup> (normalization is meant to the geometric surface area of the sample). This means that already in lab-scale experiments, the standard instrumentation (galvanostat/potentiostat) is to be equipped with current boosters. As standard boosters usually allow the control of currents up to 20 A, up-scaling may require specialized instruments as well. When using such high currents, secondary effects (such as that of Joule heat and *IR*-drop) should not be ignored, well-chosen cell geometries must be applied, and measures for electric shock protection must be taken.

## 3. Some Metal Foams Prepared by DHBT, with Potential Application in the Electroreduction of CO<sub>2</sub>

Metals suited for catalysing electrochemical CO<sub>2</sub> reduction are usually those where hydrogen evolution proceeds only at high overpotentials. These metals can exhibit a relatively broad range of potentials where CO<sub>2</sub> reduction may already occur, while water splitting still remains relatively suppressed. These metals belong, according to Winand's classification, to the group of normal or intermediate metals. A non-exhaustive list includes pure metals such as Sn<sup>[66,67]</sup> Pb,<sup>[68]</sup> Zn,<sup>[69,70]</sup> Bi,<sup>[71]</sup> Ag<sup>[72-74]</sup> and Cu,<sup>[75-78]</sup> as well as bimetallic systems where Sn foams are deposited on Cu surfaces<sup>[79-84]</sup> or when smoothly dispersed Ag and Cu form one bimetallic foam structure.<sup>[85,86]</sup> In what follows, we summarize the DHBT-assisted preparation strategies of these metal foams, as well as some important aspects of CO<sub>2</sub> reduction occurring on them.

### 3.1. Sn Foams (Pure)

Sn is a prime example of normal metals having a low melting point, little activity for HER and high activity for metal deposition. Although on a Cu substrate, Sn foams were deposited relatively early by Shin *et al.*,<sup>[29]</sup> from a bath that contained 0.15 mol dm<sup>-3</sup> SnSO<sub>4</sub> dissolved in 1.5 mol dm<sup>-3</sup> H<sub>2</sub>SO<sub>4</sub>. By applying galvanostatic deposition at a (geometric surface area normalised) current density of -3 A cm<sup>-2</sup> for 5 to 20 seconds, 100 to 300 μm thick deposits with surface pores of 100 to 400 μm diameter were obtained (Figure 9). The foam walls of Sn were composed of relatively long and dense, straight dendritic particles. The apparent microporosity (that is, the microscopic porosity of the walls of bigger pores) described in the same work by Shin *et al.*,<sup>[29]</sup> for Cu, was not seen in the case of Sn, probably as a result of the suppressed electrocatalytic activity of Sn towards HER (Figure 2).

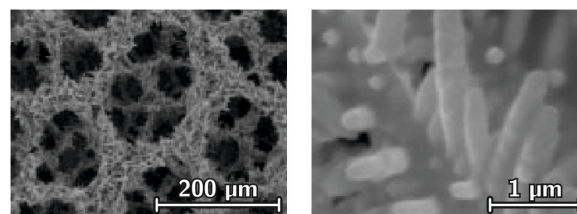


**Figure 9.** Scanning electron micrographs of a Sn foam deposited on a Cu substrate from a bath that contained 0.15 mol dm<sup>-3</sup> SnSO<sub>4</sub> dissolved in 1.5 mol dm<sup>-3</sup> H<sub>2</sub>SO<sub>4</sub> by galvanostatic electrolysis at -3 A cm<sup>-2</sup> nominal current density, lasting 5 seconds. Reproduced from Ref. 29, with the permission of Wiley.

Using a Sn instead of a Cu substrate, and SnCl<sub>2</sub> instead of SnSO<sub>4</sub> as a metal source bath component, deposits with qualities similar to those shown in Figure 9 were obtained by Du *et al.*<sup>[67]</sup> and were used for the electroreduction of CO<sub>2</sub>. They showed that compared to planar Sn electrodes, Sn foams can deliver a higher yield and better selectivity for the production of formate. In a CO<sub>2</sub>-saturated 0.1 mol dm<sup>-3</sup> NaHCO<sub>3</sub> solution, the maximum Faradaic efficiency of formate production could reach above 90% at a current density of about 23.5 mA cm<sup>-2</sup> (*E* = -1.9 V vs. SCE), which are among the highest reported to date under ambient conditions (H-type cell, aqueous solution, atmospheric pressure and room temperature).<sup>[67]</sup>

This improved production rate of formate can be attributed to the high surface area and porous structure. Moreover, Du *et al.*<sup>[67]</sup> demonstrated a high stability of their Sn foam catalyst; namely, the Faradaic efficiency remained unchanged during 16 hours of electrolysis. What cannot be inferred from Ref. 67 is, however, whether the outstanding tendencies towards the production of formate had any relation to the oxidation state of the Sn foam electrode. That oxide remnants on Sn catalysts have a guiding role in the production of formate has long been known,<sup>[66,87-89]</sup> and that surface oxidation promotes formate production (on the account of CO formation) was proven also for the case of large surface area Sn dendrites, the surface oxidation of which was induced by heating in air.<sup>[66]</sup>

### 3.2. Sn Foams (Deposited on Cu)

While reports on the use of pure Sn foams clearly point out that the large surface area of these foams lead to both a higher catalytic activity and an increased selectivity towards the production of formate,<sup>[66,67]</sup> the picture is not this clear in the case of foams composed of Sn deposited on top of Cu substrates (that is, Sn@Cu foams).

While browsing the literature, we can find works that advocate Sn@Cu foams for their excellent selectivity (> 90%) towards formate production,<sup>[79,81,82]</sup> while for some other researchers,<sup>[83,84]</sup> Sn@Cu foams seem to be of more value if the selectivity towards CO production is higher (again, > 90%). A comparison of two Sn foams deposited on Cu, with markedly different selectivities, is shown in Figure 10.



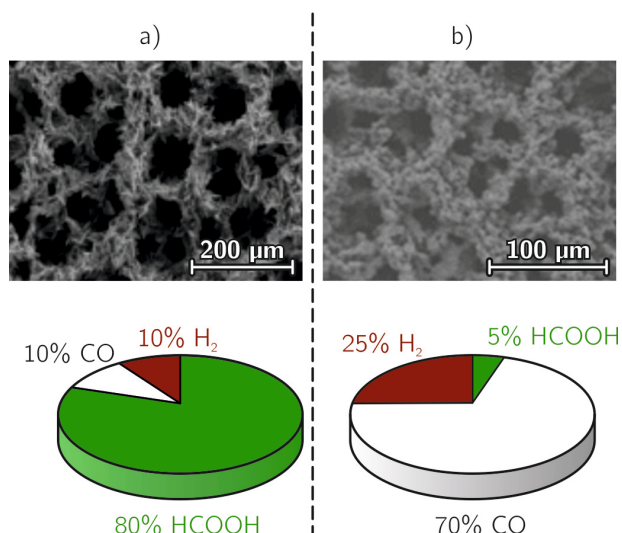


**Figure 10.** Sn foams deposited on a Cu substrate by a) Qin *et al.*<sup>[81]</sup> and b) Li *et al.*<sup>[84]</sup> Scanning electron micrographs, reproduced from Ref. 81 with the permission of Elsevier and from Ref. 84 with that of MDPI, show similar surface morphologies, yet the product distribution is markedly different, as determined for potentiostatic electrolyses at  $-1.0$  V vs. RHE in  $0.1$  mol dm $^{-3}$  CO $_2$ -saturated KHCO $_3$  solutions.

It is expected that also in case of these systems, the surface oxidation state of Sn particles has a pivotal role in determining selectivity. It was found, for example, by Li *et al.*<sup>[84]</sup> that the surface of Sn foams deposited on Cu substrates often contains SnO $_2$ . We presume that stannic (or for that matter stannous) oxide domains in Sn foams may either be incorporated in the foam structure due to the local alkalination of the electrode as a result of DHBT deposition, or that even the entire foam surface may get partly oxidised after the foam is emerged from the depositing bath, and dried in air. Either way, it was found that these electrodes exhibit an SnO $_x$  coverage-dependent catalysis – *i.e.*, a shift from CO selectivity to HCOOH selectivity with increasing SnO $_2$  coverage.<sup>[84]</sup>

We assume that in case of Sn@Cu systems, bimetallic corrosion effects may account for that some electrocatalytically active SnO $_x$  particles may survive the reductive conditions of CO $_2$  electrolysis. This may explain that, as shown in Figure 10, in some Sn@Cu foams the selectivity of formate production is preserved.

### 3.3. Pb Foams

According to Winand's classification, Pb also belongs to the group of normal metals.<sup>[49]</sup> The preparation method of Pb foams was described by Cherevko *et al.*<sup>[41]</sup> using perchloric acid both as a supporting electrolyte and an H $^+$  source. Deposition occurred on a Pt substrate from a solution containing  $0.01$  mol dm $^{-3}$  PbClO $_4$  and  $0.01$ – $1.8$  mol dm $^{-3}$  HClO $_4$ , under potentiostatic control at  $-2$  V vs. Ag | AgCl. Good porous structures were only obtained above a HClO $_4$  concentration of  $0.6$  mol dm $^{-3}$  (Figure 11). From a bath with a HClO $_4$  concen-

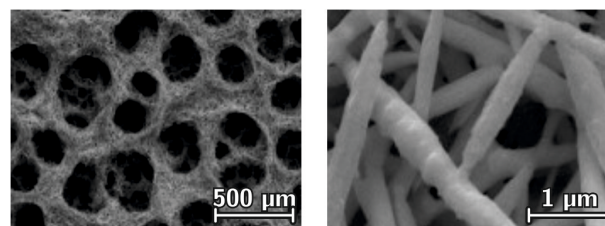


**Figure 11.** Scanning electron micrographs of a Pb foam deposited on a Pt substrate from a bath that contained  $0.01$  mol dm $^{-3}$  PbClO $_4$  dissolved in  $0.6$  mol dm $^{-3}$  HClO $_4$  by potentiostatic electrolysis lasting 2 seconds at  $-2$  V vs. Ag | AgCl. Reproduced from Ref. 41, with the permission of Elsevier.

tration of  $0.6$  mol dm $^{-3}$ , deposited Pb layers exhibited pore sizes of about  $300$   $\mu$ m. The walls of the pores showed a microstructure consisting of  $200$ – $300$  nm diameter wires at lower perchloric acid concentrations, while at higher concentrations ( $>0.9$  mol dm $^{-3}$ ) the Pb wires were either partially or fully covered by granular particles.

The above procedure was adapted by Wang *et al.*<sup>[68]</sup> in order to obtain Pb foams applicable for the electroreduction of CO $_2$ . They showed that the porous Pb foam had a better electrocatalytic performance for the production of formate than a Pb plate: at  $5$  °C, the highest recorded Faradaic efficiency of formate production was  $96.8\%$  at an applied potential of  $-1.7$  V vs. SCE in a  $0.5$  mol dm $^{-3}$  KHCO $_3$  solution saturated by CO $_2$ . In another study, Fan *et al.*<sup>[90]</sup> have shown that the selectivity towards formate seems to correlate with the proportion of surface sites with the (100) orientation.

### 3.4. Zn Foams

While also belonging to the normal group of metals, reports about the electrodeposition of Zn foams are recent. In the work of Luo *et al.*<sup>[69]</sup> Zn foams were deposited on a Cu mesh from solutions containing  $0.1$  mol dm $^{-3}$  ZnSO $_4$  and  $1.5$  mol dm $^{-3}$  (NH $_4$ ) $_2$ SO $_4$ . They applied a current density of  $-1$  A cm $^{-2}$  for 30 seconds in order to obtain the deposited Zn foam shown by the micrographs of Figure 12. These reveal macropores with an average diameter of  $30$   $\mu$ m and micropores with a diameter

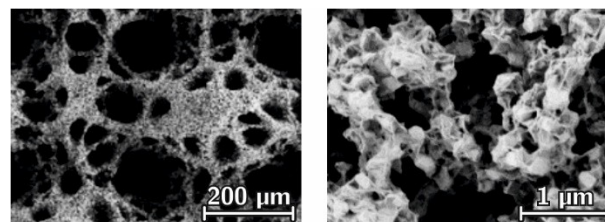


**Figure 12.** Scanning electron micrographs of a Zn foam deposited on a Pt substrate from a bath that contained  $0.1$  mol dm $^{-3}$  ZnSO $_4$  dissolved in  $1.5$  mol dm $^{-3}$  (NH $_4$ ) $_2$ SO $_4$  by galvanostatic electrolysis at  $-3$  A cm $^{-2}$  nominal current density, lasting 5 seconds. Reproduced from Ref. 69, with permission of the American Chemical Society.

smaller than 2  $\mu\text{m}$ , the latter formed as channels of the leaving, smaller  $\text{H}_2$  bubbles.

Luo *et al.*<sup>[69]</sup> investigated the electroreduction of  $\text{CO}_2$  on their highly porous Zn foam (Figure 12), and found a remarkably high Faradaic efficiency of 95% towards the formation of CO at  $E = -0.95$  V vs. RHE, where the current density was about  $-27$   $\text{mA cm}^{-2}$ , in a  $\text{CO}_2$ -purged 0.1  $\text{mol dm}^{-3}$   $\text{KHCO}_3$  electrolyte. They argued that above the overall increase of the surface area, the Zn foam also offers a large number of active surface sites (compared to Zn foils) that play a decisive role in improving the catalytic activity. At the same time, the high local pH induced by the porous structure of Zn results in an enhanced CO selectivity because of suppressed  $\text{H}_2$  evolution. Luo *et al.*<sup>[69]</sup> also transformed their Zn foam into a gas diffusion electrode, achieving a current density of 200  $\text{mA cm}^{-2}$  for the reduction of  $\text{CO}_2$  and an 84% Faradaic efficiency for CO production at  $-0.64$  V in a flow-cell reactor.

In another work,<sup>[70]</sup> we also developed a Zn-based alloy foam catalyst by the application of DHBT, using copper ions as a foaming agent and thereby obtaining an alloy with 6 atomic % copper content. We detected a  $>90\%$  Faradaic efficiency for CO production at  $-0.95$  V vs. RHE in  $\text{CO}_2$ -purged 0.5  $\text{mol dm}^{-3}$   $\text{KHCO}_3$ . The high efficiency was ascribed to the combination of high density of low coordinated active sites and preferential Zn(101) over Zn(002) texturing,<sup>[70]</sup> and we pointed out by means of X-ray photoelectron spectroscopy investigations that the actual catalyst material is shaped upon reduction of an oxide/hydroxide-terminating surface, under  $\text{CO}_2$  electrolysis conditions. In Ref. 70 we have also shown that intentional stressing by oxidation at ambient conditions proves to be beneficial for further activation of the catalyst.

### 3.5. Ag Foams

Silver is usually also considered a normal metal according to Winand's classification<sup>[49]</sup> but as long as silver is deposited not from a simple  $\text{Ag}^+$  solution but from a solution of its complexes, it is usually treated as an intermediate metal.<sup>[35]</sup>

The first reports on the DHBT fabrication of silver foams originate from Cherevko *et al.*,<sup>[37,38]</sup> and these occurred from a thiocyanate complex solution of silver. The foam structure shown in Figure 13 was obtained by potentiostatic deposition at  $-3$  V vs. Ag | AgCl lasting 30 seconds. For this deposition, Cherevko *et al.*<sup>[38]</sup> used a Pt substrate and a bath containing

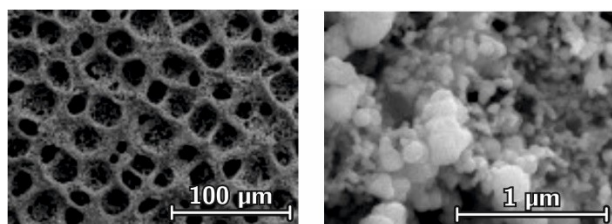


**Figure 13.** Scanning electron micrographs of an Ag foam deposited on a Pt substrate from a bath that contained 0.01  $\text{mol dm}^{-3}$   $\text{Ag}_2\text{SO}_4$ .

0.01  $\text{mol dm}^{-3}$   $\text{Ag}_2\text{SO}_4$ , 1.5  $\text{mol dm}^{-3}$  KSCN acting as a complexing agent, 0.75  $\text{mol dm}^{-3}$   $\text{NH}_4\text{Cl}$ , and 0.01  $\text{mol dm}^{-3}$  sodium citrate.  $\text{NH}_4\text{Cl}$  acted as an  $\text{H}^+$  source and the authors found that a minimum threshold concentration of  $>0.5$   $\text{mol dm}^{-3}$  of  $\text{NH}_4\text{Cl}$  is required for the deposit to show a foamy structure. A decrease in the diameter (from 45 to about 20  $\mu\text{m}$ ) and wall thickness of the surface pores, as well as an increase of the number of formed holes with increasing concentrations of  $\text{NH}_4\text{Cl}$  was observed. The authors found<sup>[38]</sup> that the microscale morphology of the formed Ag deposits changes, from exhibiting nanosized dendrites in case of foams deposited at low  $\text{NH}_4\text{Cl}$  concentrations towards small particle agglomerates, deposited from baths with higher  $\text{NH}_4\text{Cl}$  content.

As for the preparation of silver foams from normal (*i.e.*, noncomplexed) solutions, reports are relatively recent. In Ref. 72 we used a silver foil substrate and a bath containing 0.02  $\text{mol dm}^{-3}$   $\text{Ag}_2\text{SO}_4$ , 1.5  $\text{mol dm}^{-3}$   $\text{H}_2\text{SO}_4$  and 0.1  $\text{mol dm}^{-3}$  sodium citrate. Note that while the bulk of the solution was acidic enough not to allow complexation of silver by citrate, in the heavily alkaline near-electrode solution region, chelation of silver ions may occur. Silver foams obtained from citrate containing and citrate-free baths are compared in Figure 14. The thickness of the deposited foams is around 17  $\mu\text{m}$ . Compared to the citrate-free deposition process, Ag foams deposited in the presence of citrate show a more uniform macroporosity with an open-cell architecture of interconnected pores. The average diameter of the macropores is significantly smaller, compared to deposits obtained from a citrate-free solution (Figure 14). This is probably related to the effect of citrate, decreasing the stress of the liquid/gas interface (cf. to Equation (3)). As expected, the inclusion of citrate in the depositing bath formulation does not only impact the obtained

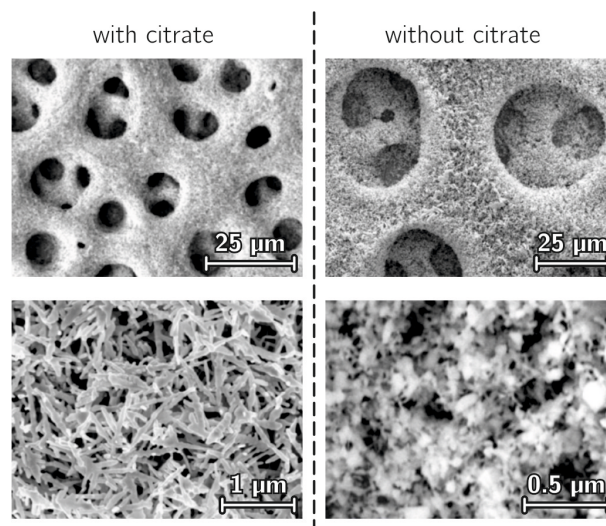


**Figure 14.** Scanning electron micrographs of an Ag foam deposited on an Ag substrate from a bath composed of 0.02  $\text{mol dm}^{-3}$   $\text{Ag}_2\text{SO}_4$  and 1.5  $\text{mol dm}^{-3}$   $\text{H}_2\text{SO}_4$ . The effect of adding sodium citrate to the bath in a 0.1  $\text{mol dm}^{-3}$  concentration can clearly be seen. Galvanostatic depositions with a nominal current density of  $-3$   $\text{A cm}^{-2}$ , lasting 20 seconds, were carried out in both cases. Reproduced from Ref. 72, with permission of the American Chemical Society.

foam morphology, but also its catalytic activity towards CO<sub>2</sub> electroreduction. Especially in terms of long-term stability, the multiporous Ag foams deposited from citrate containing baths perform better than the ones prepared from citrate-free depositing solutions.<sup>[72]</sup>

Silver foams deposited from a citrate-containing solution were used as electrocatalysts for CO<sub>2</sub> reduction. Potentiostatic electrolyses in CO<sub>2</sub>-saturated 0.5 mol dm<sup>-3</sup> KHCO<sub>3</sub> solutions were carried out in a hermetically tight H-type cell, and the partial current densities corresponding to the formation of each product were determined by means of on-line gas chromatography.<sup>[91]</sup> The potential of using silver foams as electrocatalyst materials becomes evident by comparing the catalytic properties of foams to those of a plain silver plate, as in Figure 15.<sup>[72]</sup>

There are two features of DHBT-deposited silver foams that become immediately apparent in Figure 15: *i.*) that the silver foam produces CO with a much higher activity and over a considerably broader potential region, compared to a simple silver plate; and *ii.*) that due to the foam-like structure, the diversity of products is increased, and especially at high negative potentials, some rather significant amounts of hydrocarbons (primarily methane and ethylene) are also formed. While the former feature casts the silver foam catalyst described in Ref. 72 one of the best Ag-based CO forming catalysts reported so far in the literature for aqueous environments, the latter feature deserves attention because the formation of hydrocarbons was reported before only on Cu-based electrode materials, while Ag is traditionally considered a strictly CO-forming catalyst.<sup>[92]</sup> Note here that, as proven by control experiments in Ref. 72, the colourful product palette shown in Figure 15b is not due to artefacts caused by citrate that was applied as an additive to the deposition bath.

As shown in Figure 15b, some  $-20 \mu\text{A cm}^{-2}$  partial current of CO formation can already be detected at the potential of  $-0.3 \text{ V vs. RHE}$ , while the onset potential of CO<sub>2</sub> reduction is about 300 mV more negative on planar silver surfaces. Note that onset potentials as low as  $-0.3 \text{ V vs. RHE}$  were so far only reported for gold nano-needle catalysts.<sup>[93]</sup> As the potential is set to more and more cathodic values, the overall current density rises, with CO remaining the only or at least the majority reaction product, down until  $-0.8$ , respectively to  $-1.2 \text{ V}$ .

At potentials less cathodic than  $-0.8 \text{ V vs. RHE}$ , not even hydrogen evolution is observed, unlike the case of plain surface silver electrodes, at which HER competes with CO<sub>2</sub> reduction even at low overpotentials. As a result, the CO-selectivity of the silver foam prepared in Ref. 72 is not peak-like as is the case of planar silver electrodes, but it remains constantly above 90% over a more than 900 mV broad potential range.

This superior selectivity towards the formation of CO was not met by other silver foam catalysts reported in the literature,<sup>[73,74]</sup> in particular because of differences of the foam structure at the nanoscale. In Ref. 72 we hypothesized that the highly anisotropic, needle-like structures seen in Figure 14, obtained so far only by citrate-assisted deposition, may account for the superior selectivity towards CO production by increasing the bonding strength of adsorbed CO to the catalyst surface. For example, on commercially available silver foam electrodes with grain-like microstructure, the Faradaic efficiency of CO production is generally lower, although the potential regime of CO formation is still broader than that on pristine silver plates.<sup>[74]</sup>

Another hint that underlines the pivotal role of adsorbed CO played in the mechanism is the formation of C<sub>1</sub> (methane) and, to some extent, C<sub>2</sub> (ethylene) hydrocarbons, which also necessitates an adsorbed CO intermediate.<sup>[94]</sup> Of course, apart

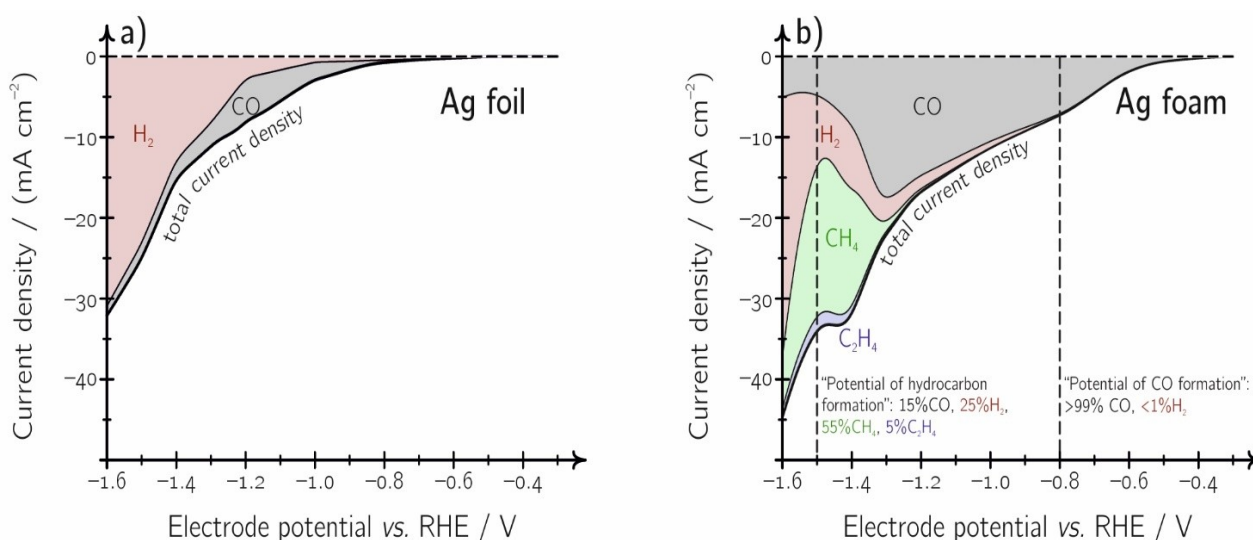


**Figure 15.** Polarization curves (interpolated) of a) a silver plate and b) the silver foam deposited from a citrate containing solution, shown in Figure 14. Electrolyses were carried out at distinct potentials in a CO<sub>2</sub>-saturated 0.5 mol dm<sup>-3</sup> KHCO<sub>3</sub> solution, and the product distribution was determined by online gas chromatography. Colour-shaded areas show the distribution of reaction products. Currents were normalized to the geometric (nominal) surface area of the electrodes. The graphs were prepared using data from Ref. 72.

from the higher bonding energy of adsorbed CO, and the longer residence time of surface-bound CO caused thereby, for the effective formation of hydrocarbons relatively intense H<sup>+</sup> reduction is also required to take place, so that surface-bound H atoms and CO molecules can effectively react.

From this point of view, the confinement of the reaction scenery to the small (macro)pores seems to be of primary importance. The hierarchical structure of the silver foam can make sure that potential intermediates (such as surface-bound CO or H<sub>2</sub>) may not easily leave the electrode surface (and become a product), but instead get entrapped in the pores, at least for some time, having a higher chance to recombine.

The effect of confinement is illustrated by Figure 16a, showing a cavity of diameter  $d$  in contact with its surroundings through an opening of diameter  $a$  and length  $L$ . By theoretical studies on the random walk of a particle inside this cavity, it was shown by Berezhkovskii *et al.*<sup>[95]</sup> that the  $\tau_{\text{res}}$  characteristic time of residence (*i.e.*, the average time a molecule would spend inside the void before diffusing out through the neck) can well be approximated using the simple formula

$$T_{\text{res}} = \frac{2d^3 L}{3a^2 D} \quad (4)$$

where  $D$  denotes the diffusion coefficient of the molecule.

Further taking into account that the characteristic time between two molecule-to-wall collisions can well be approximated as

$$T_{\text{coll}} = \frac{d^2}{6D} \quad (5)$$

it can be assumed that an average molecule, after born and before leaving the void, collides

$$N_{\text{coll}} = \frac{T_{\text{res}}}{T_{\text{coll}}} = \frac{4dL}{a^2} \quad (6)$$

times to the surface of the cavity. Using the arbitrary (but, based on the morphology shown for example in Figure 14, not unrealistic) parameter set of  $d = 50 \mu\text{m}$ ,  $a = 25 \mu\text{m}$ ,  $L = 50 \mu\text{m}$  and  $D = 5 \cdot 10^{-6} \text{cm}^2 \text{s}^{-1}$ , we get to a residence time of about 13 seconds, during which a formed molecule would impact about 16 times the wall of the cavity, having ample opportunity to re-adsorb, and act further as an intermediate.

As seen in Equations (4) and (6), the characteristic residence time and the mean collision number increases with the  $L$  length of the neck that separates the cavity from its surroundings. This hints to that the confinement effect in case of deep-buried cavities is bigger. For near-surface cavities (for which  $L \approx 0$ ), another work of Berezhkovskii *et al.*<sup>[96]</sup> provides the formula

$$T_{\text{res}} = \frac{d^3 \pi}{12aD} \quad (7)$$

for the residence time, from which an average collision number

$$N_{\text{coll}} = \frac{d\pi}{2a} \quad (8)$$

follows. Using the above-mentioned parameters, the obtained residence time and collision number are about an order of magnitude smaller compared to when the escape occurs through a finite length neck. The concept is further illustrated by Figure 16b, showing the presumed Langevin trajectory<sup>[97]</sup> of a particle being formed and moving inside a void, before leaving it through an opening.

Although the above arguments are very simple and rather qualitative in nature, they well explain the effect of small-scale confinement on electrocatalytic processes. It is assumed that the above "multi-collision" effect is what lies behind the possibility of the formation of C<sub>2</sub> products on Ag foams, and a similar argument is often used for explaining CO<sub>2</sub> electro-reduction mechanisms on-going on Cu electrodes, allowing even the formation of C<sub>3</sub> products.<sup>[98]</sup>

One has to note, however, that the Ag foam catalyst described in Ref. 72, although it is one of the most excellent

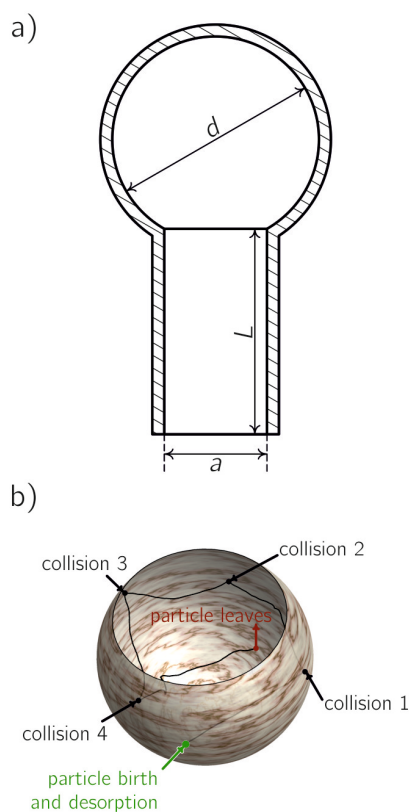


**Figure 16.** a) A spherical cavity of diameter  $d$ , connected to its surroundings by a neck with length  $L$  and diameter  $a$ . b) Simulated motion of a particle inside a spherical segment. After formed, the particle leaves the surface of the cavity and begins to traject, hitting in this case, four times the cavity wall before eventually leaving the void.

catalyst material for CO production, is not the ideal playground for hydrocarbon formation. While it was observed that when operated on a long run at potentials of CO formation (see Figure 15b) the catalyst performs well without any significant degradation effects, as electrolyses are carried out at more negative potentials to form hydrocarbons, the performance of the catalyst decreases over time. This probably has to do with the poisoning of the silver foam by the formed methane, and can also be related to a mechanical degradation caused by the intensive gas evolution observed during long-lasting electrolyses.

In order to study degradation effects, we used identical location scanning electron microscopy<sup>[99]</sup> in Ref. 72. Figure 17 demonstrates degradation suffered by silver foams over long times of electrolyses at potentials where hydrocarbons are formed. Note here also, that long-lasting electrolysis at CO-forming potential does not cause any visible degradation of the catalyst.

From point of view of future applications of Ag foams in CO-producing electrolyzers, it also seems important in particular for future studies to fine-tune the foam preparation procedure in the direction of obtaining well-structured foams on sub-

strates that are more challenging than a plain Ag foil. Deposition on gas diffusion electrodes (GDEs) seems to be a logical first step of up-scaling attempts. During our pilot studies in this direction, we found that the Ag foam preparation recipe mentioned before (and described in details in Ref. 72) needs further improvement, as it yields a less well-defined foam structure when we apply it for the deposition of Ag foams on GDEs (compare Figure 18a to Figure 14). Nonetheless, even though there is obviously space for further development, Ag foams on GDEs exhibit a superior activity towards CO formation, as shown by results of our recent (yet unpublished) investigations (Figure 18b).

### 3.6. Cu Foams

As opposed to silver and to the other metals discussed above, copper is usually considered as the only metal where the formation of C<sub>1</sub> (methane and methanol), C<sub>2</sub> (ethylene and ethyl-alcohol), or even C<sub>3</sub> products (propyl-alcohol) is possible, even if the applied catalyst is not of a foam structure.<sup>[92]</sup>

Several studies were conducted in the past with the aim of understanding the selectivity of Cu catalysts towards the formation of certain products.<sup>[75–78,94,100–107]</sup> These studies all

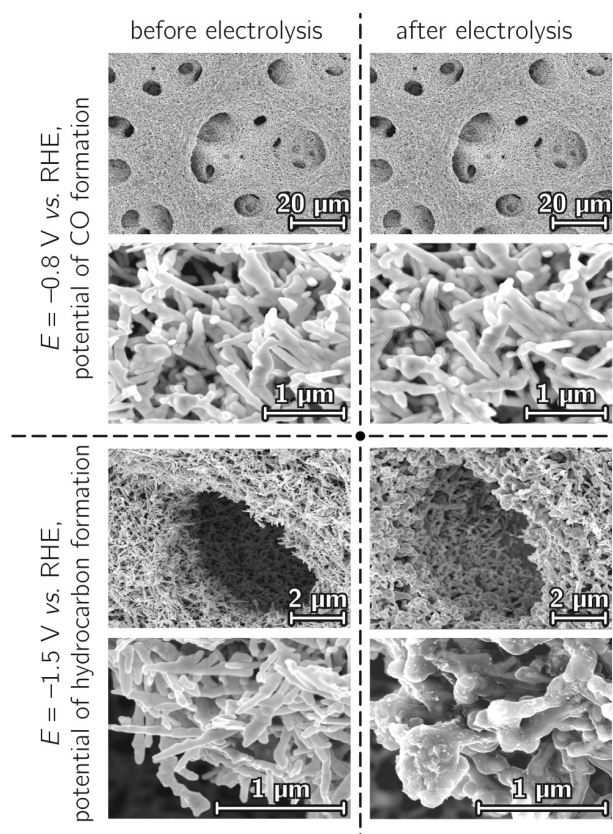


**Figure 17.** Scanning electron micrographs recorded at identical locations of an Ag foam catalyst, before and after being used for some hours for the electroreduction of CO<sub>2</sub>. Mild potentials, where only CO is formed, cause no significant damage; however, long-time polarization in the range of extreme negative potentials where hydrocarbons are formed causes visible degradation, especially on the nanoscale.

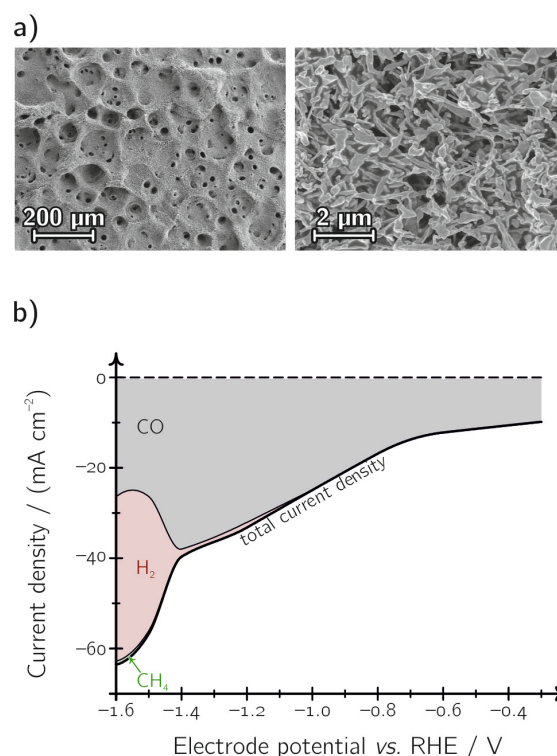


**Figure 18.** a) Scanning electron micrographs of a silver foam deposited by 20 s electrolysis using the recipe described in Ref. 72 onto a Sigracet 39 BC gas diffusion electrode (Fuel Cell Store). b) Interpolated product distribution and total current density plot measured on the GDE by electrolyses carried out in an H-type cell at distinct potentials in a CO<sub>2</sub>-saturated 0.5 mol dm<sup>-3</sup> KHCO<sub>3</sub> solution. (Unpublished data)

underline the importance of the bonding strength between the catalyst surface and the  $\cdot\text{CO}_2^-$  radical anion that, following a coupled  $\text{H}^+/\text{e}^-$  (alternatively, direct adsorbed H) transfer, forms surface-bound CO, which acts as a second key intermediate.<sup>[75]</sup> By contrast to some other metals previously mentioned in this study, copper can bond CO strongly enough to allow its further reduction to  $\text{C}_1$ ,  $\text{C}_2$  or even to  $\text{C}_3$  products. Both experimental<sup>[100]</sup> and theoretical investigations<sup>[104]</sup> indicate that C–C coupling is more probable on (100) oriented copper surfaces while the  $\text{C}_1$  pathway is preferential on the (111) surface.<sup>[75]</sup> As a result, significant effort (relying on the use of sputtering and electropolishing<sup>[103]</sup> as well as electrodeposition and anodization techniques<sup>[108]</sup>) has recently been devoted to find possibilities of tuning Cu surfaces towards the right (preferably,  $\text{C}_2$ ) selectivity. Amongst these approaches, the oxidation of the copper surface,<sup>[105–107]</sup> yielding weakly coordinated structures, seems to be the most promising. Note here, however, that the thus obtained catalysts should not be referred to as copper oxide, but rather as oxide derived (OD) copper catalysts, since under the heavily cathodic operating conditions, the copper oxide is instantaneously reduced to an elementary Cu state.

In a recent paper,<sup>[75]</sup> we combined the activation of Cu catalysts via the reduction of its surface oxide with the DHBT-based foam deposition approach first developed by Shin *et al.*<sup>[30]</sup> We thus produced mesoporous, large surface area copper foams, shown in Figure 19. Several procedures for the potentiostatic (Figures 3 and 4) and galvanostatic (Figure 5) means of copper foam preparation were reported by the works of Nikolić *et al.*<sup>[31–36]</sup> and of Zhang *et al.*<sup>[52]</sup> These works, and the mechanistic description of copper foam deposition described therein, were reviewed here in the section before.

For purposes of  $\text{CO}_2$  electrolysis, our group used galvanostatic deposition (nominal current density:  $-3 \text{ A cm}^{-2}$ ) to deposit black copper foams on a Cu wafer substrate from a

bath that contained  $0.2 \text{ mol dm}^{-3} \text{ CuSO}_4$  and  $1.5 \text{ mol dm}^{-3} \text{ H}_2\text{SO}_4$ . As seen in Figure 19, deposits with a hierarchical macroporosity were obtained, with macropore sizes growing as a function of deposition time. The thus prepared Cu foams underwent a fast surface oxidation, following emersion from the plating bath. We demonstrated that these OD Cu foam catalysts show a superior selectivity toward  $\text{C}_2$  product formation at particularly low overpotentials.<sup>[75]</sup>

In Figure 20 the electrocatalytic properties of the copper foam deposited with a 20 s deposition time are compared to those of a planar Cu wafer. Both surfaces exhibit a clear preference for hydrocarbon formation, in combination with a significantly reduced preference for formate production. Whereas on the Cu wafer methane is the primary product, the  $\text{C}_2$  pathway seems to prevail on the Cu foam catalyst, with the  $\text{C}_1$  pathway suppressed to such extent that not even traces of methane formation are detected.

The preference of OD Cu foams towards the  $\text{C}_2$  pathway can probably be explained by two, synergistic effects: *i.*) that the OD Cu surface is composed more of (100) oriented (open) facets<sup>[75]</sup> and *ii.*) that due to the porous structure (confinement), key intermediates of the  $\text{C}_2$  pathway may be entrapped and get readsorbed inside the catalyst pores. The latter effect is demonstrated by Figure 21, showing an anti-correlated variation of the Faradaic efficiencies of  $\text{C}_2$  products and that of CO, as a function of the surface pore size of the copper foam catalyst.

With regard to the microscopic structure of the OD copper foam catalysts, we note that while thermal annealing can aid in the oxidation of the foam surface (and by altering the surface morphology, it may result in FE variations), the thus formed oxide is almost immediately reduced to elementary copper under the harsh cathodic conditions applied for  $\text{CO}_2$  electrolysis, and has thus no role in the  $\text{CO}_2$  reduction mechanism. The

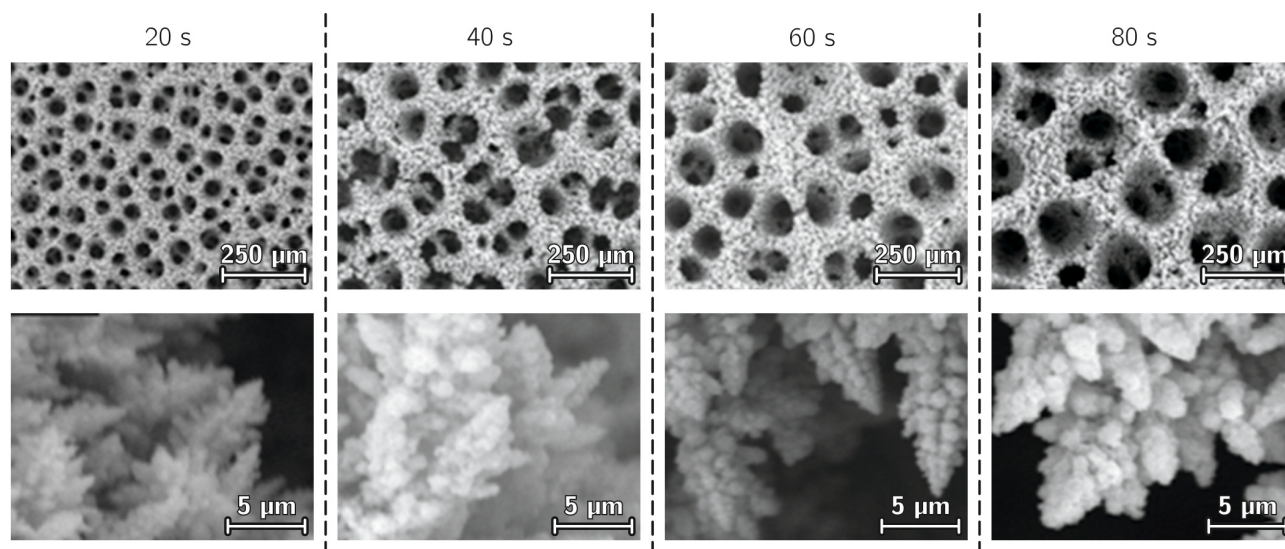


**Figure 19.** Scanning electron micrographs of Cu foams, deposited galvanostatically (nominal current density:  $-3 \text{ A cm}^{-2}$ ) on a Cu wafer from a bath that contained  $0.2 \text{ mol dm}^{-3} \text{ CuSO}_4$  and  $1.5 \text{ mol dm}^{-3} \text{ H}_2\text{SO}_4$ . Deposits obtained with different electrolysis times are shown. Reproduced from Ref. 75, with permission of the American Chemical Society.

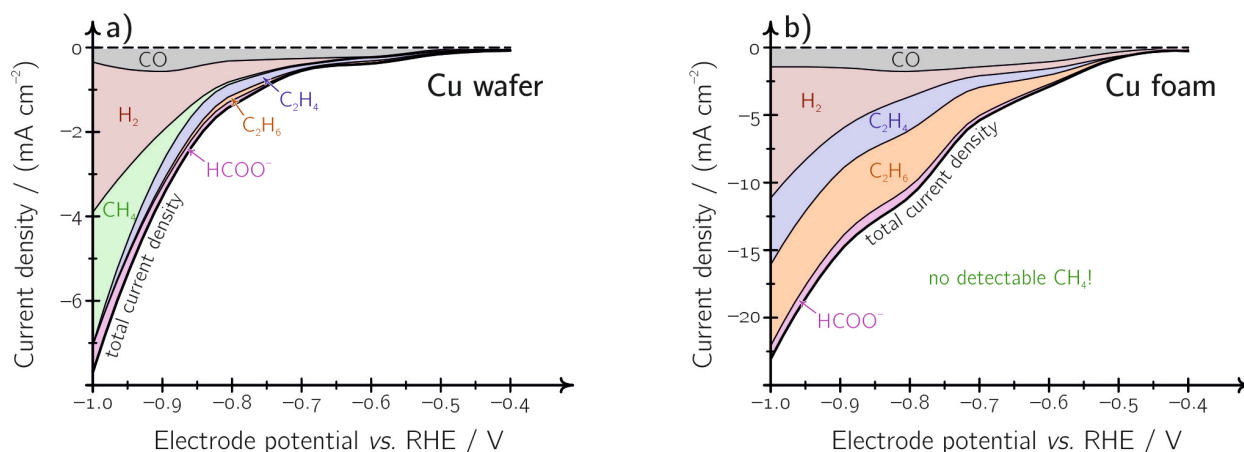


**Figure 20.** Polarization curves (interpolated) of a) a copper wafer and b) the copper foam shown in Figure 14 with the deposition time of 20 s. Electrolyses were carried out at distinct potentials in a  $\text{CO}_2$ -saturated  $0.5 \text{ mol dm}^{-3} \text{ NaHCO}_3$  solution, and the product distribution was determined by online gas, as well as post-electrolysis ionic liquid chromatography. Colour-shaded areas show the distribution of reaction products. Currents were normalized to the geometric (nominal) surface area of the electrodes. The graphs were prepared using data from Ref. 75.

disappearance (reduction) of surface copper oxides on Cu foam catalysts was recently proven by a combined operando X-ray diffraction (XRD), X-ray absorption spectroscopy (XAS) and Raman spectroscopy study.<sup>[76]</sup>

### 3.7. Ag–Cu Bimetallic Foams

By the combination of (primarily, CO forming) silver and (primarily,  $\text{C}_2$  hydrocarbons forming) copper sites in the form of one bimetallic metal foam, it seems possible to direct the electroreduction of  $\text{CO}_2$  towards the formation of products even

more desired than either CO or hydrocarbons: ethyl- or even propylalcohol.<sup>[86]</sup>

The DHBT co-deposition of Ag–Cu bimetallic foams were first reported by Najdovski *et al.*,<sup>[46]</sup> who applied galvanostatic  $|j| > 1 \text{ A cm}^{-2}$  co-depositions in  $\text{H}_2\text{SO}_4$ -acidified baths that contained both  $\text{CuSO}_4$  and  $\text{AgNO}_3$ . As expected,<sup>[109]</sup> no alloy formation was observed and Najdovski *et al.* showed that the Ag–Cu bimetallic foam consists of small segregates of silver and copper phases.<sup>[46]</sup>

They observed that the surface pore size obtained during codeposition increases with increasing the  $c_{\text{Ag}^+} : c_{\text{Cu}^{2+}}$  ratio of the depositing bath. They argued that the increase of surface pore diameters, as well as the appearance of surface crack lines at higher silver contents is due to Ag exhibiting less catalytic activity towards HER than Cu (Figure 2), which favours the coalescence of  $\text{H}_2$  bubbles.

The recipe of Najdovski *et al.*<sup>[46]</sup> was later applied by Kottakkat *et al.*<sup>[85]</sup> in order to create bimetallic Ag–Cu foams for purposes of  $\text{CO}_2$  electroreduction. They used constant current ( $-1 \text{ A cm}^{-2}$ , 10 s) co-deposition from baths containing  $0.2 \text{ mol dm}^{-3} \text{ CuSO}_4$ ,  $1.5 \text{ mol dm}^{-3} \text{ H}_2\text{SO}_4$  and  $0.01$ – $0.05 \text{ mol dm}^{-3} \text{ AgNO}_3$ . Kottakkat *et al.*<sup>[85]</sup> observed an improved CO selectivity and suppression of hydrogen evolution at low overpotentials, when comparing their bimetallic Ag–Cu foams to a plain Ag foil, and, similarly, a decrease of the Faradaic efficiency of formate production, compared to Cu foams.<sup>[85]</sup> The overall increase of the CO selectivity of bimetallic Ag–Cu foams was explained by an increased bonding strength of adsorbed CO, that Kottakkat *et al.*<sup>[85]</sup> verified by operando Raman spectroscopy. Although for other Ag–Cu bimetallic systems an enhanced selectivity towards multi-carbon oxygenate products was detected,<sup>[110]</sup> and it was attributed to near-surface alloying due to mechanical strain,<sup>[111]</sup> the formation of  $\text{C}_2$  products, especially that of alcohols, was not observed by Kottakkat *et al.* on their Ag–Cu foams.<sup>[85]</sup>

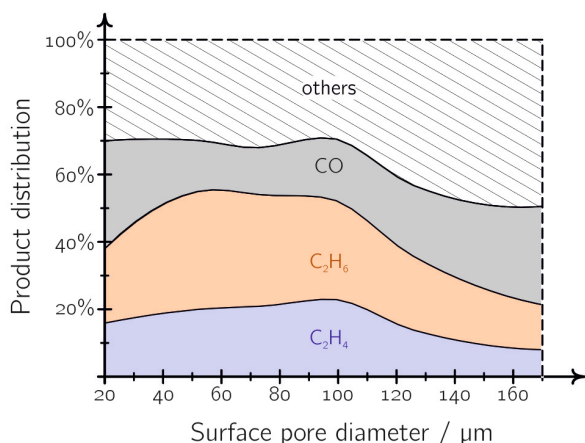


**Figure 21.** The distribution of  $\text{CO}_2$  reduction products depend on the surface pore size of the Cu foam catalyst. Potentiostatic electrolyses lasting 1 hour were conducted at a potential of  $-0.8 \text{ V}$  vs. RHE in a  $\text{CO}_2$ -saturated  $0.5 \text{ mol dm}^{-3} \text{ NaHCO}_3$  solution, and main gaseous products were analysed by means of online gas chromatography. Colour-shaded areas show the distribution of reaction products. The graph was prepared using data from Ref. 75.

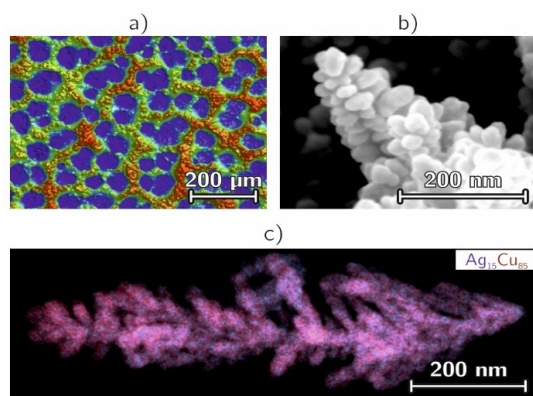


Figure 22. An Ag–Cu bimetallic foam deposited galvanostatically

In Ref. 86 we modified the original bath formulation of Najdovski *et al.*<sup>[46]</sup> by the inclusion of sodium citrate that, acting both as an adsorbent and a local chelating agent, changed the deposition mechanism,<sup>[86]</sup> resulting in honeycomb-like macropores and a fine dendritic microscopic structure. This is shown in Figure 22 for an Ag<sub>15</sub>Cu<sub>85</sub> bimetallic foam deposited galvanostatically ( $j = -3 \text{ A cm}^{-2}$ ,  $t = 20 \text{ s}$ ) on a Cu foil substrate from a bath containing  $1.5 \text{ mol dm}^{-3} \text{ H}_2\text{SO}_4$ ,  $0.02 \text{ mol dm}^{-3} \text{ CuSO}_4$ ,  $0.002 \text{ mol dm}^{-3} \text{ AgNO}_3$  and  $0.1 \text{ mol dm}^{-3}$  sodium citrate.

Note that the notation Ag<sub>15</sub>Cu<sub>85</sub> is based on an ICP–OES determination of the (bulk) atomic composition and by no means reflects compound formation. The white-light interferometric image of the Ag–Cu foam in Figure 22a reveals a near-surface pore diameter of  $\sim 25 \mu\text{m}$ ; note, however, that the pore diameter is expected to vary also in this case along the surface normal, as was shown for other foams before (Figure 7). The side-walls of the macropores reveal dendrites with dimensions  $< 50 \text{ nm}$ , as shown in the electron micrograph of Figure 22b.

The dendrites themselves are composed of small, individual Ag and Cu phases, as revealed by the energy-dispersive X-ray map in Figure 22c.

The electrocatalytic performance of Ag<sub>15</sub>Cu<sub>85</sub> bimetallic foams was investigated in Ref. 86 by 1 hour long electrolysis experiments carried out at certain potentials in CO<sub>2</sub>-saturated  $0.5 \text{ mol dm}^{-3} \text{ KHCO}_3$  solutions. Results of these electrolysis experiments are shown in Figure 23.a.

It can be seen in Figure 23a that within the range of low overpotentials ( $-0.7 \text{ V} < E < -0.3 \text{ V}$  vs. RHE) the predominant CO<sub>2</sub> reduction product is CO, assumed to take place preferentially on the Ag sites of the bimetallic catalyst. Accordingly, the Faradaic efficiency of formate production is suppressed, especially when compared to Cu foams, and in agreement with the observations of Kottakkat *et al.*<sup>[85]</sup> made on other bimetallic Ag–Cu foams. At potentials more cathodic than  $-0.5 \text{ V}$  vs. RHE, hydrogen formation sets on, and along with it, pathways for the production of methane, ethylene and some small amounts ( $< 1\%$ ) of ethane are opened.<sup>[86]</sup> At  $E < -0.7 \text{ V}$ , the product distribution of CO<sub>2</sub> reduction is already obviously dominated by the Cu component, as C–C coupling reactions are enabled. It can be assumed, that the C–C coupling reaction benefits from the high abundance of CO inside the porous catalyst. Due to the small domain sizes of the metallic components of the as-deposited Ag<sub>15</sub>Cu<sub>85</sub> foam, the CO intermediate is rapidly transported from the Ag (CO producer) to the Cu domains (C–C coupler), either by surface diffusion (“spill-over”) or by diffusion through the liquid electrolyte phase inside the pores of the bimetallic foam (as depicted in Figure 16b). As shown in Figure 23a, CO<sub>2</sub> reduction already results in the formation of some little amount of ethanol at this potential range, while only traces of *n*-propanol are detected.

The product distribution becomes remarkably different if we make subject the deposited Ag<sub>15</sub>Cu<sub>85</sub> foam to thermal annealing before it is used as an electrocatalyst of CO<sub>2</sub>

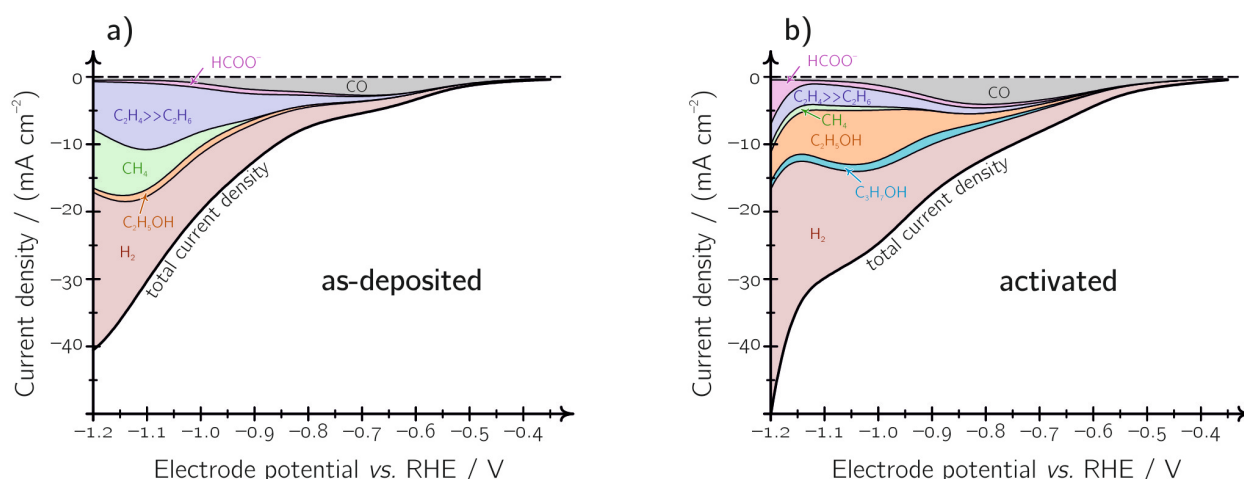
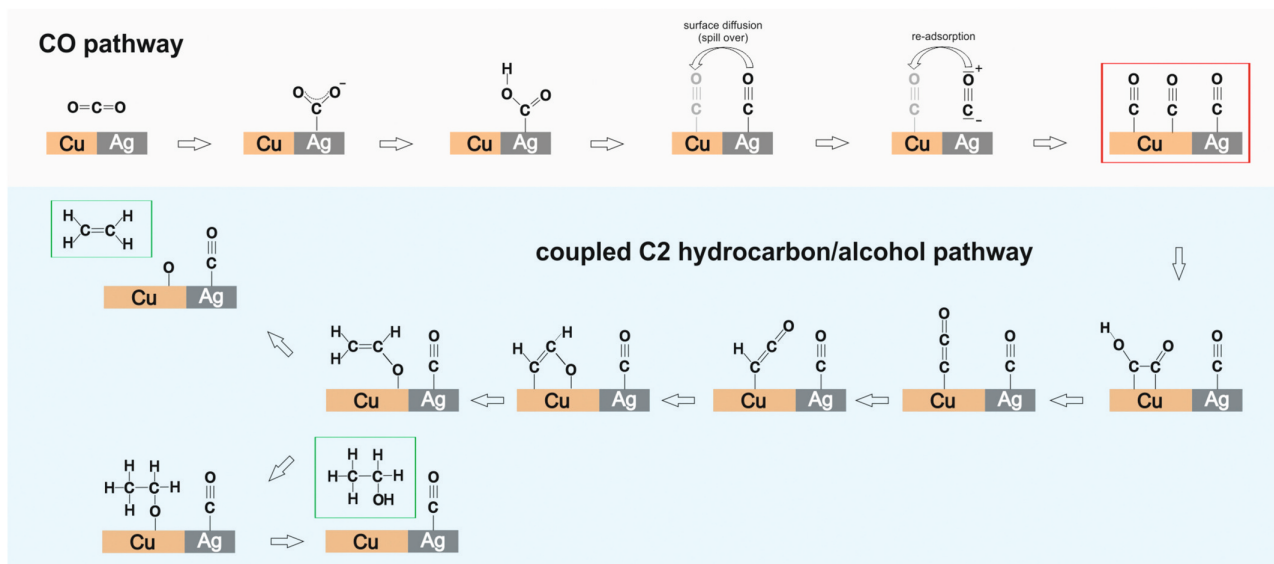


Figure 23. Polarization curves (interpolated) of CO<sub>2</sub> reduction recorded on a) an as-deposited Ag<sub>15</sub>Cu<sub>85</sub> bimetallic foam and b) on the same foam following activation by mild thermal annealing in air ( $200^\circ\text{C}$ , 12 hours). Electrolyses were carried out at distinct potentials in a CO<sub>2</sub>-saturated  $0.5 \text{ mol dm}^{-3} \text{ KHCO}_3$  solution, and the product distribution was determined by online gas, as well as by post-electrolysis ionic liquid chromatography. Colour-shaded areas show the distribution of reaction products. Currents were normalized to the geometric (nominal) surface area of the electrodes. The graphs were prepared using data from Ref. 86.





**Figure 24.** Proposed reaction scheme illustrating the coupling of the CO pathway and the C<sub>2</sub> hydrocarbon/alcohol reaction pathways on oxide-derived Ag<sub>15</sub>Cu<sub>85</sub> bimetallic foams. Reproduced from Ref. 86 with the permission of Elsevier.

reduction (Figure 23b). It was shown in Ref. 86 that thermal annealing under mild conditions (200 °C for 12 hours) transforms the Cu in the bimetallic system into a mixture of crystalline Cu<sub>2</sub>O and amorphous CuO, whereas the Ag islands remain in a metallic state due to the thermal instability of Ag<sub>2</sub>O above temperatures of 180 °C. The selective oxidation of Cu in the bimetallic Ag<sub>15</sub>Cu<sub>85</sub> catalyst goes along with an enrichment of Cu oxides on the surface of the formed mixed AgCu<sub>x</sub>O foam. Although both *operando* X-ray diffraction and *operando* Raman spectroscopy confirm that the cuprous/cupric oxide content of the catalyst is reduced back to the metallic state at potentials applied for CO<sub>2</sub> electrolysis, the formed oxide-derived bimetallic Ag–Cu foam was found to exhibit high selectivity towards alcohol formation (Figure 23b), with Faradaic efficiencies of about 34% and 7% for ethanol and *n*-propanol formation, respectively.

Extended electrolysis experiments (100 h) indicated a superior degradation resistance of the oxide-derived bimetallic catalyst, which was ascribed to the effective suppression of the C<sub>1</sub> hydrocarbon reaction pathway, assuring that irreversible carbon contaminations, appearing in particular during methane production, can be avoided.

The suggested mechanism of alcohol formation on the oxide derived, bimetallic Ag–Cu foam catalyst surface is shown in Figure 24. This mechanism is consistent with published models on alcohol formation on Cu,<sup>[112]</sup> with the addition that on the bimetallic foam CO forms selectively on the Ag domains, and is subsequently transported to the Cu domains via surface diffusion (“spillover”) or alternatively via CO transport through the solution phase (desorption/readsorption). Besides the increased abundance of CO intermediates, it is the stabilization of the chemisorbed CO on the catalyst surface which further directs CO<sub>2</sub> reduction towards C–C coupling and alcohol formation, as confirmed by *operando* Raman experiments.<sup>[86]</sup>

### 3.8. Multimetallic Foams

The combination of multiple (more than two) metals in one foam structure has recently emerged as a new possibility of electrocatalyst design. In 2019 Lee *et al.*<sup>[113]</sup> described a Cu–In–Ag foam that was created by the deposition of a Cu foam that was electroplated by In and further modified by partial galvanic replacement of In with Ag (Figure 25). The preparation method is described briefly in Table 1, details can be found in Ref. 113. By the use of this trimetallic foam, Lee *et al.* achieved high Faradaic efficiency of CO production already at low overpotentials that, as they argued, was a result of synergistic effects arising from the high surface area of the Cu foam, the HER suppressing effect of In, and by Ag as a CO

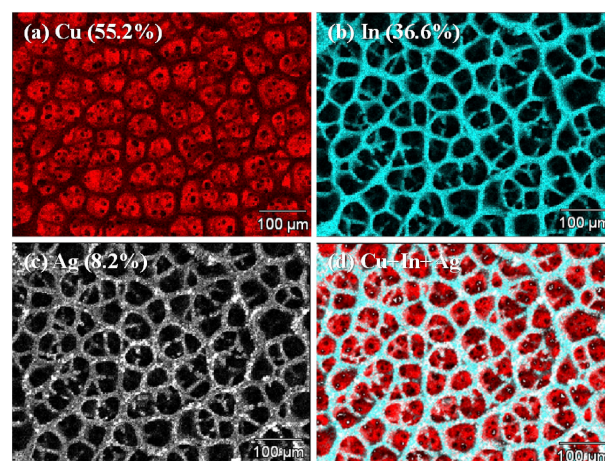


**Figure 25.** Elemental energy dispersive spectroscopy maps of the Ag–In–Cu foam prepared by Lee *et al.*<sup>[113]</sup> (a) Cu, (b) In, (c) Ag, and (d) Cu + In + Ag. Reproduced from Ref. 113, with the permission of Elsevier.

**Table 1.** Overview of the metal foams (preparation and CO<sub>2</sub> reduction characteristics) discussed in Section 3.

Metal (featured CO <sub>2</sub> reduction product)	Preparation using the DHBT technique	CO <sub>2</sub> reduction characteristics
Sn, pure (formate) <sup>[67]</sup>	0.15 mol dm <sup>-3</sup> SnSO <sub>4</sub> , 1.5 mol dm <sup>-3</sup> H <sub>2</sub> SO <sub>4</sub> , galvanostatic deposition on Sn foil, typ. current density: -3 A cm <sup>-2</sup> , typ. deposition time: 5 to 20 s.	In CO <sub>2</sub> -sat. 0.1 mol dm <sup>-3</sup> NaHCO <sub>3</sub> , at E = -1.9 V vs. SCE <i>j</i> ≈ -23.5 mA cm <sup>-2</sup> ; > 90% FE for formate production.
Sn@Cu (formate) <sup>[81]</sup>	0.1 mol dm <sup>-3</sup> SnCl <sub>2</sub> , 0.1 mol dm <sup>-3</sup> sodium citrate, 1.2 mol dm <sup>-3</sup> HCl, galvanostatic deposition on electro-polished Cu foil, typ. current density: -2 A cm <sup>-2</sup> , typ. deposition time: 2 min.	In CO <sub>2</sub> -sat. 0.1 mol dm <sup>-3</sup> KHCO <sub>3</sub> , at E = -1.2 V vs. RHE <i>j</i> ≈ -6.5 mA cm <sup>-2</sup> ; > 90% FE for formate production.
Pb (formate) <sup>[68]</sup>	0.01 mol dm <sup>-3</sup> PbClO <sub>4</sub> , 0.01 mol dm <sup>-3</sup> sodium citrate, 1.0 mol dm <sup>-3</sup> HClO <sub>4</sub> , galvanostatic deposition on Pb plate, typ. current density: -0.5 to -8 A cm <sup>-2</sup> , typ. deposition time: 10 to 20 s.	In CO <sub>2</sub> -sat. 0.5 mol dm <sup>-3</sup> KHCO <sub>3</sub> , at E = -1.7 V vs. SCE <i>j</i> ≈ -10 mA cm <sup>-2</sup> ; > 97% FE for formate production at 5 °C.
Zn (CO) <sup>[69]</sup>	0.1 mol dm <sup>-3</sup> ZnSO <sub>4</sub> , 1.5 mol dm <sup>-3</sup> (NH <sub>4</sub> ) <sub>2</sub> SO <sub>4</sub> , galvanostatic deposition on a Cu mesh, typ. current density: -1 A cm <sup>-2</sup> , typ. deposition time: 30 s.	In CO <sub>2</sub> -sat. 0.1 mol dm <sup>-3</sup> KHCO <sub>3</sub> , at E = -0.95 V vs. SCE <i>j</i> ≈ -27 mA cm <sup>-2</sup> ; > 95% FE for CO formation.
Ag (CO) <sup>[72]</sup>	0.02 mol dm <sup>-3</sup> Ag <sub>2</sub> SO <sub>4</sub> , 0.1 mol dm <sup>-3</sup> sodium citrate, 1.5 mol dm <sup>-3</sup> H <sub>2</sub> SO <sub>4</sub> , galvanostatic deposition on an Ag foil, typ. current density: -3 A cm <sup>-2</sup> , typ. deposition time: 20 s.	In CO <sub>2</sub> -sat. 0.5 mol dm <sup>-3</sup> KHCO <sub>3</sub> , at E = -0.8 V vs. RHE about -8 mA cm <sup>-2</sup> ; > 99% FE for CO formation. At E = -1.5 V vs. RHE <i>j</i> ≈ -36 mA cm <sup>-2</sup> ; FEs: 15% CO, 25% H <sub>2</sub> , 55% CH <sub>4</sub> , 5% C <sub>2</sub> H <sub>4</sub> .
Cu (C <sub>2</sub> hydrocarbons) <sup>[75]</sup>	0.2 mol dm <sup>-3</sup> CuSO <sub>4</sub> , 1.5 mol dm <sup>-3</sup> H <sub>2</sub> SO <sub>4</sub> , galvanostatic deposition on a Cu wafer, typ. current density: -3 A cm <sup>-2</sup> , typ. deposition time: 20 s. See Ref..	In CO <sub>2</sub> -sat. 0.5 mol dm <sup>-3</sup> KHCO <sub>3</sub> , at E = -0.8 V vs. RHE <i>j</i> ≈ -12 mA cm <sup>-2</sup> ; FEs: 37% C <sub>2</sub> H <sub>6</sub> , 22% C <sub>2</sub> H <sub>4</sub> , 16% CO, 7% HCOOH, 17% H <sub>2</sub> . See Ref. 75.
CuAg bimetallic (C <sub>2</sub> alcohols) <sup>[86]</sup>	0.02 mol dm <sup>-3</sup> CuSO <sub>4</sub> , 0.002 mol dm <sup>-3</sup> AgNO <sub>3</sub> , 1.5 mol dm <sup>-3</sup> H <sub>2</sub> SO <sub>4</sub> , galvanostatic deposition on a Cu foil, typ. current density: -3 A cm <sup>-2</sup> , typ. deposition time: 20 s, activated by annealing in air at 200 °C, 12 hours.	In CO <sub>2</sub> -sat. 0.5 mol dm <sup>-3</sup> KHCO <sub>3</sub> , at E = -1.05 V vs. RHE <i>j</i> ≈ -27 mA cm <sup>-2</sup> ; FEs: 28% C <sub>2</sub> H <sub>5</sub> OH, 4% C <sub>3</sub> H <sub>7</sub> OH, 10% C <sub>2</sub> hydrocarbons, 2.5% formate, 2.5% CH <sub>4</sub> , 3% CO, 50% H <sub>2</sub> .
AgInCu trimetallic (CO) <sup>[113]</sup>	Cu foam substrate is prepared from 0.12 mol dm <sup>-3</sup> CuSO <sub>4</sub> , 0.5 mol dm <sup>-3</sup> H <sub>2</sub> SO <sub>4</sub> , 1.2 mol dm <sup>-3</sup> (NH <sub>4</sub> ) <sub>2</sub> SO <sub>4</sub> and 40 μmol dm <sup>-3</sup> benzotriazole on a Ti foil, galvanostatically, at a current density of -1.2 A cm <sup>-2</sup> for 40 s. In deposition then takes place on the Cu foam at a current density of -50 mA cm <sup>-2</sup> for 900 s, in a 0.1 mol dm <sup>-3</sup> InCl <sub>3</sub> and 0.5 mol dm <sup>-3</sup> HClO <sub>4</sub> solution. Galvanic replacement by Ag follows by immersion into a solution of 10 mmol dm <sup>-3</sup> AgNO <sub>3</sub> and 2 mmol dm <sup>-3</sup> 2-nitrobenzoic acid.	In CO <sub>2</sub> -sat. 0.5 mol dm <sup>-3</sup> KHCO <sub>3</sub> , at E = -0.53 V vs. RHE <i>j</i> ≈ -2 mA cm <sup>-2</sup> ; > 74% FE for CO formation.

producer. Apart from minor amounts of formate produced, Lee *et al.* did not detect any products other than CO and H<sub>2</sub> on this trimetallic foam.

#### 4. Summary and Outlook

In this review we attempted to provide an oversight on the current state-of-the-art of DHBT-based deposition of metal foams, and on the application of these materials as promising new catalysts of the electroreduction of CO<sub>2</sub>.

We gave an introduction to the phenomenology and mechanism of DHBT-based deposition of metal foams, addressing the most important factors affecting the structure and surface morphology of the prepared foams. It was shown that by a careful selection of appropriate experimental parameters, foams of hierarchical structure can be created from various types of noble, intermediate and normal metals. The success of DHBT-based foam deposition depends on a set of parameters, and appropriate selection of the applied (potentiostatic/galvanostatic) mode of deposition, the value of the electrode potential or current at which the deposition is carried out, as well as the proper formulation of the depositing bath have a key impact on the deposited foam structure. With respect to bath formulation, most emphasis is laid on the concentration of the used metal salt and of the acid component, as well as on

the concentration of buffering or complexing agents, and that of surfactants.

The review contains a brief description of several recipes, originating from works of our own or that of other groups, for the deposition of some metal foams, including pure metals such as Sn, Pb, Zn, Ag, Cu, as well as two-component systems like Sn foams deposited on Cu and the mixed Ag–Cu bimetallic foam. The reason why these metal foams and not some others like Pt, Pd, or Au were made subject of this study, is that the mentioned metals are the most promising candidates to be used as catalyst materials in electrochemical CO<sub>2</sub> reduction.

Accordingly, foams prepared by the DHBT technique from the above metals were also discussed from the point of view of CO<sub>2</sub> reduction, by placing special emphasis on the product distribution of this versatile process. While it is usually noted that on metal foams, mostly due to their increased surface area, electrocatalytic processes can occur at a higher rate compared to plain electrodes of the same metal, we found that hierarchical metal foams prepared by the DHBT technique often have a lot more to offer.

As it was pointed out especially in the cases of Ag, Cu and Ag–Cu bimetallic foams, the pores of these hierarchical three-dimensional structures can harbour reactions which would otherwise be unavailable on open surfaces due to the confinement (entrapping) of key reaction intermediates. In case of CO<sub>2</sub> electroreduction, confinement allows desorbed CO and H<sub>2</sub> to remain close and potentially re-adsorb on the electrode surface,

ultimately leading to the formation of reaction products of a lower oxidation state (such as hydrocarbons and alcohols). Moreover, by the application of post-deposition, pre-electrolysis treatments (such as the oxidation of Cu-containing foams by annealing in air), the microstructure of the foams may further be fine-tuned towards the formation of certain, desired, CO<sub>2</sub> reduction products. Although most metal oxides never survive the reductive conditions of CO<sub>2</sub> electrolysis, oxide-derived surfaces have a different (usually, more open) structure, which opens a pathway before the formation of C<sub>2</sub> and even of C<sub>3</sub> products.

To conclude, the DHBT technique of metal foams preparation has the key advantage of meeting the most important structural and electronic factors that are considered essential for the electrocatalysis of CO<sub>2</sub> reduction. Processes fundamental to the technique, such as bubble nucleation, growth and detachment mechanisms, as well as the kinetics of metal deposition and dendrite formation are now understood at a level which will allow the rational design of mono- or multi-metallic foams that can act as new catalysts of CO<sub>2</sub> reduction. As it was shown, research on some metal foam catalysts is now ready to move in the direction of industrial upscaling (cf. to Figure 18), as foams with good structural qualities can even be deposited on gas diffusion electrodes. It is thus expected that in the coming years, metal foams will provide a viable alternative to, and may even outperform supported nanoparticle based (ink-like) catalysts in terms of yield, selectivity and, especially, stability.

## Acknowledgements

Support by the CTI Swiss Competence Center for Energy Research (SCCER Heat and Electricity Storage) is gratefully acknowledged. P. B. acknowledges financial support from the Swiss National Foundation (grant 200020-172507). S. V. acknowledges support from the National Research, Development and Innovation Office of Hungary (NKFIH grants PD124079 and FK135375).

## Conflict of Interest

The authors declare no conflict of interest.

**Keywords:** power-to-value · CO<sub>2</sub> reduction · Faradaic efficiency · selectivity · confinement

- [1] S. J. Davis, K. Caldeira, H. D. Matthews, *Science* **2010**, *329*, 1330–1333.
- [2] B. Khezri, A. C. Fisher, M. Pumera, *J. Mater. Chem. A* **2017**, *5*, 8230–8246.
- [3] F. D. Meylan, V. Moreau, S. Erkman, *J. CO<sub>2</sub> Util.* **2015**, *12*, 101–108.
- [4] W. Luc, F. Jiao, *ACS Catal.* **2017**, *7*, 5856–5861.
- [5] P. Liu, G. Chen, *Porous Materials*, Butterworth-Heinemann, Oxford, **2014**, pp. 189–220.
- [6] W. Zhu, R. Zhang, F. Qu, A. M. Asiri, X. Sun, *ChemCatChem* **2017**, *9*, 1721–1743.
- [7] H. Zhao, Y.-P. Zhu, Z.-Y. Yuan, *Eur. J. Inorg. Chem.* **2016**, *2016*, 1916–1923.

- [8] *IUPAC Compendium of Chemical Terminology* (Eds.: A. D. McNaught, A. Wilkinson), Blackwell Scientific Publications, Oxford, 2<sup>nd</sup> ed, **1997**.
- [9] R. Du, X. Jin, R. Hübner, X. Fan, Y. Hu, A. Eychmüller, *Adv. Energy Mater.* **2020**, *10*, 1901945.
- [10] M. F. Ashby, T. Evans, N. A. Fleck, J. W. Hutchinson, H. N. G. Wadley, *Metal Foams: A Design Guide*, Butterworth-Heinemann, **2000**.
- [11] H. W. Pickering, P. R. Swann, *Corrosion* **1963**, *19*, 373–389.
- [12] K. Hashimoto, T. Goto, W. Suëtaka, S. Shimodaira, *Trans. Jpn. Inst. Met.* **1965**, *6*, 107–112.
- [13] A. J. Forty, *Nature* **1979**, *282*, 597–598.
- [14] J. Erlebacher, M. J. Aziz, A. Karma, N. Dimitrov, K. Sieradzki, *Nature* **2001**, *410*, 450–453.
- [15] D. Walsh, L. Arcelli, T. Ikoma, J. Tanaka, S. Mann, *Nat. Mater.* **2003**, *2*, 386–390.
- [16] H.-L. Gao, L. Xu, F. Long, Z. Pan, Y.-X. Du, Y. Lu, J. Ge, S.-H. Yu, *Angew. Chem. Int. Ed.* **2014**, *53*, 4561–4566; *Angew. Chem.* **2014**, *126*, 4649–4654.
- [17] B. C. Tappan, M. H. Huynh, M. A. Hiskey, D. E. Chavez, E. P. Luther, J. T. Mang, S. F. Son, *J. Am. Chem. Soc.* **2006**, *128*, 6589–6594.
- [18] B. C. Tappan, S. A. Steiner, E. P. Luther, *Angew. Chem. Int. Ed.* **2010**, *49*, 4544–4565; *Angew. Chem.* **2010**, *122*, 4648–4669.
- [19] N. C. Bigall, A.-K. Herrmann, M. Vogel, M. Rose, P. Simon, W. Carrillo-Cabrera, D. Dorfs, S. Kaskel, N. Gaponik, A. Eychmüller, *Angew. Chem. Int. Ed.* **2009**, *48*, 9731–9734; *Angew. Chem.* **2009**, *121*, 9911–9915.
- [20] W. Liu, A.-K. Herrmann, N. C. Bigall, P. Rodriguez, D. Wen, M. Oezaslan, T. J. Schmidt, N. Gaponik, A. Eychmüller, *Acc. Chem. Res.* **2015**, *48*, 154–162.
- [21] S. Tang, S. Vongehr, Y. Wang, J. Cui, X. Wang, X. Meng, *J. Mater. Chem. A* **2014**, *2*, 3648–3660.
- [22] B. J. Plowman, L. A. Jones, S. K. Bhargava, *Chem. Commun.* **2015**, *51*, 4331–4346.
- [23] O. Lummer, F. Kurlbaum, *Ann. Phys. Chem.* **1892**, *282*, 204–224.
- [24] F. Kohlrausch, *Ann. Phys. Chem.* **1897**, *299*, 423–430.
- [25] S. E. Stanca, F. Hänschke, A. Ihring, G. Zieger, J. Dellith, E. Kessler, H.-G. Meyer, *Sci. Rep.* **2017**, *7*, 1074.
- [26] *Modern Electroplating* (Eds.: M. Schlesinger, M. Paunovic), Wiley, New York, 5<sup>th</sup> ed, **2010**.
- [27] C. Marozzi, A. Chialvo, *Electrochim. Acta* **2000**, *45*, 2111–2120.
- [28] C. Marozzi, A. Chialvo, *Electrochim. Acta* **2001**, *46*, 861–866.
- [29] H.-C. Shin, J. Dong, M. Liu, *Adv. Mater.* **2003**, *15*, 1610–1614.
- [30] H.-C. Shin, M. Liu, *Chem. Mater.* **2004**, *16*, 5460–5464.
- [31] N. D. Nikolić, K. I. Popov, Lj. J. Pavlović, M. G. Pavlović, *J. Electroanal. Chem.* **2006**, *588*, 88–98.
- [32] N. Nikolić, K. Popov, Lj. Pavlović, M. Pavlović, *Sensors* **2007**, *7*, 1–15.
- [33] N. Nikolić, G. Branković, M. Pavlović, K. Popov, *J. Electroanal. Chem.* **2008**, *621*, 13–21.
- [34] N. D. Nikolić, K. I. Popov, *Mod. Aspects Electrochem.*, Springer, New York, **2010**, pp. 1–70.
- [35] N. D. Nikolić, *Morphology of Electrochemically and Chemically Deposited Metals*, Springer, Cham, **2016**, pp. 171–203.
- [36] N. D. Nikolić, *J. Electrochem. Sci. Eng.* **2020**, *10*, 111–126.
- [37] S. Cherevko, X. Xing, C.-H. Chung, *Electrochem. Commun.* **2010**, *12*, 467–470.
- [38] S. Cherevko, C.-H. Chung, *Electrochim. Acta* **2010**, *55*, 6383–6390.
- [39] S. Cherevko, C.-H. Chung, *Talanta* **2010**, *80*, 1371–1377.
- [40] S. Cherevko, C.-H. Chung, *Electrochem. Commun.* **2011**, *13*, 16–19.
- [41] S. Cherevko, X. Xing, C.-H. Chung, *Appl. Surf. Sci.* **2011**, *257*, 8054–8061.
- [42] S. Cherevko, N. Kulyk, C.-H. Chung, *Nanoscale* **2012**, *4*, 568–575.
- [43] S. Cherevko, N. Kulyk, C.-H. Chung, *Nanoscale* **2012**, *4*, 103–105.
- [44] I. Najdovski, P. R. Selvakannan, A. P. O'Mullane, S. K. Bhargava, *Chem. Eur. J.* **2011**, *17*, 10058–10063.
- [45] A. Ott, L. A. Jones, S. K. Bhargava, *Electrochem. Commun.* **2011**, *13*, 1248–1251.
- [46] I. Najdovski, P. R. Selvakannan, A. P. O'Mullane, *RSC Adv.* **2014**, *4*, 7207.
- [47] V. E. Coyle, D. K. J. Oppedisano, L. A. Jones, A. E. Kandjani, Y. M. Sabri, S. K. Bhargava, *J. Electrochem. Soc.* **2016**, *163*, B689–B695.
- [48] M. de J. Gálvez-Vázquez, V. Grozovski, N. Kovács, P. Broekmann, S. Vesztegom, *J. Phys. Chem. C* **2020**, *124*, 3988–4000.
- [49] R. Winand, *Electrochim. Acta* **1994**, *39*, 1091–1105.
- [50] S. Trasatti, *J. Electroanal. Chem. Interfacial Electrochem.* **1972**, *39*, 163–184.
- [51] Y. Li, Y.-Y. Song, C. Yang, X.-H. Xia, *Electrochem. Commun.* **2007**, *9*, 981–988.
- [52] H. Zhang, Y. Ye, R. Shen, C. Ru, Y. Hu, *J. Electrochem. Soc.* **2013**, *160*, D441–D445.

- [53] K. Popov, S. S. Djokić, B. Grgur, *Fundamental Aspects of Electro-metallurgy*, Springer, New York, 2013.
- [54] N. Ibl, *Chem. Ing. Tech.* **1961**, *33*, 69–74.
- [55] P. Chandran, S. Bakshi, D. Chatterjee, *Chem. Eng. Sci.* **2015**, *138*, 99–109.
- [56] L. J. J. Janssen, J. G. Hoogland, *Electrochim. Acta* **1970**, *15*, 1013–1023.
- [57] H. Vogt, R. J. Balzer, *Electrochim. Acta* **2005**, *50*, 2073–2079.
- [58] N. Kovács, V. Grozovski, P. Moreno-García, P. Broekmann, S. Vesztergom, *J. Electrochem. Soc.* **2020**, *167*, 102510.
- [59] D. Fernández, P. Maurer, M. Martine, J. M. D. Coey, M. E. Möbius, *Langmuir* **2014**, *30*, 13065–13074.
- [60] W. Fritz, *Phys. Z.* **1935**, *36*, 379–384.
- [61] G. G. Láng, C. A. Barbero, *Laser Techniques for the Study of Electrode Processes*, Springer, Berlin, 2012, pp. 41–73.
- [62] S. A. Amadi, D. R. Gabe, M. Goodenough, *J. Appl. Electrochem.* **1991**, *21*, 1114–1119.
- [63] H. Yang, X. Hao, J. Tang, W. Jin, C. Liu, H. Hou, X. Ji, J. Hu, *Appl. Surf. Sci.* **2019**, *494*, 731–739.
- [64] Y. Li, W.-Z. Jia, Y.-Y. Song, X.-H. Xia, *Chem. Mater.* **2007**, *19*, 5758–5764.
- [65] N. L. Ritzert, T. P. Moffat, *J. Phys. Chem. C* **2016**, *120*, 27478–27489.
- [66] D. H. Won, C. H. Choi, J. Chung, M. W. Chung, E.-H. Kim, S. I. Woo, *ChemSusChem* **2015**, *8*, 3092–3098.
- [67] D. Du, R. Lan, J. Humphreys, S. Sengodan, K. Xie, H. Wang, S. Tao, *ChemistrySelect* **2016**, *1*, 1711–1715.
- [68] J. Wang, H. Wang, Z. Han, J. Han, *Front. Chem.* **2015**, *9*, 57–63.
- [69] W. Luo, J. Zhang, M. Li, A. Züttel, *ACS Catal.* **2019**, *9*, 3783–3791.
- [70] P. Moreno-García, N. Schlegel, A. Zanetti, A. C. López, M. de Jesús Gálvez-Vázquez, A. Dutta, M. Rahaman, P. Broekmann, *ACS Appl. Mater. Interfaces* **2018**, *10*, 31355–31365.
- [71] M. Fan, S. Prabhudev, S. Garbarino, J. Qiao, G. A. Botton, D. A. Harrington, A. C. Tavares, D. Guay, *Appl. Catal. B* **2020**, *274*, 119031.
- [72] A. Dutta, C. E. Morstein, M. Rahaman, A. Cedeño López, P. Broekmann, *ACS Catal.* **2018**, *8*, 8357–8368.
- [73] H. Wang, Z. Han, L. Zhang, C. Cui, X. Zhu, X. Liu, J. Han, Q. Ge, *J. CO<sub>2</sub> Util.* **2016**, *15*, 41–49.
- [74] Y. Yu, N. Zhong, J. Fang, S. Tang, X. Ye, Z. He, S. Song, *Catal.* **2019**, *9*, 57.
- [75] A. Dutta, M. Rahaman, N. C. Luedi, M. Mohos, P. Broekmann, *ACS Catal.* **2016**, *6*, 3804–3814.
- [76] A. Dutta, M. Rahaman, B. Hecker, J. Drnec, K. Kiran, I. Z. Montiel, D. J. Weber, A. Zanetti, A. C. López, I. Martens, P. Broekmann, M. Oezaslan, *J. Catal.* **2020**.
- [77] S. Sen, D. Liu, G. T. R. Palmore, *ACS Catal.* **2014**, *4*, 3091–3095.
- [78] S. Min, X. Yang, A.-Y. Lu, C.-C. Tseng, M. N. Hedhili, L.-J. Li, K.-W. Huang, *Nano Energy* **2016**, *27*, 121–129.
- [79] Y. Wang, J. Zhou, W. Lv, H. Fang, W. Wang, *Appl. Surf. Sci.* **2016**, *362*, 394–398.
- [80] W. Lv, J. Zhou, F. Kong, H. Fang, W. Wang, *Int. J. Hydrogen Energy* **2016**, *41*, 1585–1591.
- [81] B. Qin, H. Wang, F. Peng, H. Yu, Y. Cao, *J. CO<sub>2</sub> Util.* **2017**, *21*, 219–223.
- [82] C. Chen, Y. Pang, F. Zhang, J. Zhong, B. Zhang, Z. Cheng, *J. Mater. Chem. A* **2018**, *6*, 19621–19630.
- [83] J. Zeng, K. Bejtka, W. Ju, M. Castellino, A. Chiodoni, A. Sacco, M. A. Farkhondehfar, S. Hernández, D. Rentsch, C. Battagliaand, C. F. Pirri, *Appl. Catal. B* **2018**, *236*, 475–482.
- [84] Q. Li, M. Li, S. Zhang, X. Liu, X. Zhu, Q. Ge, H. Wang, *Catalysts* **2019**, *9*, 476.
- [85] T. Kottakkat, K. Klingan, S. Jiang, Z. P. Jovanov, V. H. Davies, G. A. M. El-Nagar, H. Dau, C. Roth, *ACS Appl. Mater. Interfaces* **2019**, *11*, 14734–14744.
- [86] A. Dutta, I. Z. Montiel, R. Erni, K. Kiran, M. Rahaman, J. Drnec, P. Broekmann, *Nano Energy* **2020**, *68*, 104331.
- [87] Y. Chen, M. W. Kanan, *J. Am. Chem. Soc.* **2012**, *134*, 1986–1989.
- [88] A. Dutta, A. Kuzume, M. Rahaman, S. Vesztergom, P. Broekmann, *ACS Catal.* **2015**, *5*, 7498–7502.
- [89] A. Dutta, A. Kuzume, V. Kaliginedi, M. Rahaman, I. Sinev, M. Ahmadi, B. R. Cuenya, S. Vesztergom, P. Broekmann, *Nano Energy* **2018**, *53*, 828–840.
- [90] M. Fan, S. Garbarino, G. A. Botton, A. C. Tavares, D. Guay, *J. Mater. Chem. A*, **2017**, *5*, 20747–20756.
- [91] A. Rudnev in *Encyclopedia of Interfacial Chemistry* (Ed.: K. Wandelt), Elsevier, Amsterdam, **2018**, pp. 321–325.
- [92] Y. Hori, *Modern Aspects of Electrochemistry*, Vol. 42, Springer, New York, **2008**, pp. 89–189.
- [93] W. Zhu, Y.-J. Zhang, H. Zhang, H. Lv, Q. Li, R. Michalsky, A. Peterson, S. Sun, *J. Am. Chem. Soc.* **2014**, *136*, 16132–16135.
- [94] R. Kortlever, J. Shen, K. J. P. Schouten, F. Calle-Vallejo, M. T. M. Koper, *J. Phys. Chem. Lett.* **2015**, *6*, 4073–4082.
- [95] A. M. Berezkhovskii, A. V. Barzykin, V. Y. Zitserman, *J. Chem. Phys.* **2009**, *130*, 245104.
- [96] I. V. Grigoriev, Y. A. Makhnovskii, A. M. Berezkhovskii, V. Y. Zitserman, *J. Chem. Phys.* **2002**, *116*, 9574–9577.
- [97] N. G. van Kampen, *Stochastic Processes in Physics and Chemistry*, Elsevier, Amsterdam **2007**.
- [98] T.-T. Zhuang, Y. Pang, Z.-Q. Liang, Z. Wang, Y. Li, C.-S. Tan, J. Li, C. T. Dinh, P. D. Luna, P.-L. Hsieh, T. Burdyny, H.-H. Li, M. Liu, Y. Wang, F. Li, A. Proppe, A. Johnston, D.-H. Nam, Z.-Y. Wu, Y.-R. Zheng, A. H. Ip, H. Tan, L.-J. Chen, S.-H. Yu, S. O. Kelley, D. Sinton, E. H. Sargent, *Nat. Can.* **2018**, *1*, 946–951.
- [99] N. Hodnik, M. Zorko, M. Bele, S. Hočevar, M. Gaberšček, *J. Phys. Chem. C*, **2012**, *116*, 21326–21333.
- [100] Y. Hori, I. Takahashi, O. Koga, N. Hoshi, *J. Mol. Catal. A* **2003**, *199*, 39–47.
- [101] K. J. P. Schouten, Y. Kwon, C. J. M. van der Ham, Z. Qin, M. T. M. Koper, *Chem. Sci.* **2011**, *2*, 1902.
- [102] K. P. Kuhl, E. R. Cave, D. N. Abram, T. F. Jaramillo, *Energy Environ. Sci.* **2012**, *5*, 7050.
- [103] W. Tang, A. A. Peterson, A. S. Varela, Z. P. Jovanov, L. Bech, W. J. Durand, S. Dahl, J. K. Nørskov, I. Chorkendorff, *Phys. Chem. Chem. Phys.* **2012**, *14*, 76–81.
- [104] J. H. Montoya, C. Shi, K. Chan, J. K. Nørskov, *J. Phys. Chem. Lett.* **2015**, *6*, 2032–2037.
- [105] C. S. Chen, J. H. Wan, B. S. Yeo, *J. Phys. Chem. C* **2015**, *119*, 26875–26882.
- [106] K. W. Frese, *J. Electrochem. Soc.* **1991**, *138*, 3338.
- [107] C. W. Li, M. W. Kanan, *J. Am. Chem. Soc.* **2012**, *134*, 7231–7234.
- [108] M. Le, M. Ren, Z. Zhang, P. T. Sprunger, R. L. Kurtz, J. C. Flake, *J. Electrochem. Soc.* **2011**, *158*, E45–E49.
- [109] P. R. Subramanian, J. H. Perepezko, *J. Phase Equilib.* **1993**, *14*, 62–75.
- [110] E. L. Clark, C. Hahn, T. F. Jaramillo, A. T. Bell, *J. Am. Chem. Soc.* **2017**, *139*, 15848–15857.
- [111] J. L. Stevens, R. Q. Hwang, *Phys. Rev. Lett.* **1995**, *74*, 2078–2081.
- [112] M. Rahaman, A. Dutta, A. Zanetti, P. Broekmann, *ACS Catal.* **2017**, *7*, 7946–7956.
- [113] H. Lee, J. Kim, I. Choi, S. H. Ahn, *Electrochim. Acta* **2019**, *323*, 133102.

Manuscript received: July 13, 2020  
Revised manuscript received: September 15, 2020  
Accepted manuscript online: November 3, 2020  
Version of record online: November 23, 2020